Journal of Medicinal Chemistry

Article

Rational Design, Synthesis and Pharmacological Characterization of Novel Ghrelin Receptor Inverse Agonists as Potential Treatment against Obesity-related Metabolic Diseases

Antoine Daina, claudio giuliano, Claudio Pietra, Junbo Wang, Yushi Chi, Zack Zou, Fugang Li, Zhonghua Yan, Yifan Zhou, Angelo Guainazzi, Silvina Garcia Rubio, and Vincent Zoete

J. Med. Chem., **Just Accepted Manuscript** • DOI: 10.1021/acs.jmedchem.8b00794 • Publication Date (Web): 28 Sep 2018

ACS Publications

is published by the American Chemical Society. 1155 Sixteenth Street N.W., Washington, DC 20036

Rational Design, Synthesis and Pharmacological Characterization of Novel Ghrelin Receptor Inverse Agonists as Potential Treatment against Obesity-related Metabolic Diseases.

Antoine Daina[1], Claudio Giuliano[2], Claudio Pietra*[2], Junbo Wang[3], Yushi Chi[3], Zack Zou[3], Fugang Li[4], Zhonghua Yan[4], Yifan Zhou[4], Angelo Guainazzi[5], Silvina Garcia Rubio[5,#], Vincent Zoete*[1,6]*

[1]Molecular Modeling Group, SIB Swiss Institute of Bioinformatics, CH-1015 Lausanne, Switzerland

[2]Research and Preclinical Development Department, Helsinn Healthcare, CH-6912 Lugano, Switzerland

[3]Department of Medicinal Chemistry, Pharmacokinetics and Metabolism, Sundia MediTech, 388 Jialilue Road, Zhangjiang Hi-Tech Park, Shanghai 201203, China

[4]Department of Discovery Biology, HD Biosciences, 590 Ruiqing Road Zhangjiang East Campus, Shanghai 201201, China

[5]Research and Development Department, Helsinn Therapeutics (US), Inc., Iselin, NJ 08830, United-States

[6] Department of Fundamental Oncology, Lausanne University, Ludwig Institute for Cancer Research, Route de la Corniche 9A, 1066 Epalinges, Switzerland

[#]Present address: Bridge Medicines, Belfer Research Building, 413 East 69th Street, New York, NY 10021, United-States

KEYWORDS

Ghrelin, GHSR, ghrelin receptor, inverse agonist, obesity, diabetes, metabolic diseases

ABSTRACT

A new chemotype of ghrelin inverse agonists was discovered through chimeric design based on molecular scaffolds known as growth-hormone secretagogue receptor (GHSR) modulators but with divergent pharmacodynamic and pharmacokinetic properties. The structure-activities/properties exploration led to compound **47**, which displayed potent human GHSR antagonism and inverse agonism in cellular assays (IC_{50} = 68 nM, EC_{50} = 29 nM), moderate oral bioavailability and notable brain penetration in rat (F = 27 %, B/P ratio = 1.9). First *in vivo* studies demonstrated effective reduction of food intake after oral or parenteral administration to mouse (78% at 1 h and 38% at 8 h, respectively). Further preclinical studies are needed to evaluate the most suited mode of administration with the aim of promoting a first central-acting ghrelin inverse agonist molecule to development, which would represent a significant step towards therapeutic agents to treat metabolic disorders related to obesity, such as type-2 diabetes mellitus.

INTRODUCTION

The growth hormone secretagogue receptor (GHSR, Uniprot ID Q92847) is a seven-transmembrane G-protein coupled receptor (GPCR) discovered in 1996.[1] While mainly found in the pituitary gland, GHSR is widely distributed across tissues, including pancreas and regions of the brain linked with energy homeostasis and feeding.[2] A remarkable quality of GHSR is its ability to adopt an active conformation without the need of an agonistic ligand. Accordingly, a

high constitutive activity can be measured on the receptor, autonomous from any ligand binding, of about half of its maximum signaling activity.[3]

Ghrelin was first described in 1999. This hormone is a 28-residue peptide, whose serine at position 3 requires an octanoylation for ghrelin to develop as the effective endogenous agonistic ligand of GHSR.[4] The first five residues at the N-terminus of the peptide (sequence: FLSPE) mostly explains molecular recognition by and activation of GHSR.[5] Ghrelin, sometime called the 'hunger hormone', is essentially implicated in the control of food intake and energy homeostasis.[6] It is secreted by endocrine cells in the stomach during fasting and prior to meals, while circulating concentrations are lowered by feeding or glucose intake.[7,8] Ghrelin was described to foster food intake and adiposity both in rodent and human.[7,9] When administrated to human or rodent, ghrelin decreases insulin release and leads to insulin resistance.[10,11] Also ghrelin-deficient mice were observed to secret more insulin with higher protection against glucose intolerance induced by fat diet. [11] In the liver, ghrelin promotes the expression of specific gluconeogenic enzymes and thus down-regulates insulin signaling.[12] Finally, ghrelin induces enzymatic lipogenic activity and inhibits lipid oxidation in white adipose tissue.[13,14]

In principle, the ghrelin pathway offers great therapeutic opportunities to treat a broad spectrum of metabolic disorders. In particular, the high constitutive activity of the receptor lays the biological rational for an investigation of ghrelin receptor inverse agonists (GHSR-IA) with anticipated higher *in vivo* efficacy than pure antagonists against obesity-related metabolic diseases. [15]

In 2003, Holst *et al*.[3] described an engineered substance P with potent inverse ghrelin effect, but the first small molecule GHSR-IA series was reported by Merck in 2009.[16] Later other groups from industry and academia published GHSR-IA of diverse chemotypes.[17-22] As shown in

Figure 1, these molecules tend to be large (MW > 500 g/mol), positively charged and to bear numerous polar moieties. The fairly extended topological polar surface areas (TPSA)[23] reflect the difficulty for these compounds to permeate through the blood-brain barrier (BBB). Moreover all compounds except **1** are predicted substrates of the P-glycoprotein 1 (P-gp) efflux pump by a support vector machine (SVM) classification model available through the swissADME web tool.[24] In fact, only compounds **3**, **6** and **7** have been measured in sufficient concentration in the brain when administrated at high dose in rodent to make them interesting preclinical central agents.

Some physiological effects of ghrelin and other GHSR agonists were shown to be peripherally mediated,[25] however, the transport through BBB proven for the acetylated ghrelin together with the high level of GHSR expression in the brain argue for significant CNS role of ghrelin.[26-28] By comparing *in vivo* effect of compound **7** and a brain non-permeant (more polar) analog of the same series (MW: 549.02 g/mol; TPSA: 110.81 $Å^2$), it was concluded that a peripheral inverse agonist can achieve reduction of food intake but weight-loss requires a CNS penetrant GHSR-IA.[22] Recently, Abegg *et al.*[29] performed a battery of *in vitro*, *in cellulo* and *in vivo* experiments to investigate thoroughly two undisclosed GHSR-IA molecules. At cellular level, immunohistochemical studies established a clear relationship between ghrelin inverse activity and reduced c-Fos response in mouse brain neurons after oral or subcutaneous administration.

Further in the same article,[29] the complete beneficial impact of GHSR-IA on energy balance and glucose homeostasis was confirmed by two different animal models.

All GHSR-IAs disclosed so far do not display sufficient access to the CNS to be promoted as centrally acting experimental drugs. In fact, the only ghrelin antagonist/inverse agonist, which has completed preclinical investigations to enter clinical phases is compound **4**, a Pfizer non-

CNS investigational drug tagged PF-05190457,[30] whose pharmacokinetic optimization rational was said to target peripheral GHSR.[19] PF-05190457 was shown to increase glucose-stimulated insulin secretion in human isolated pancreatic islets and thus is anticipated in the diabetes mellitus therapeutic area.[31] Recently, a study in healthy individuals reported high tolerability and pharmacokinetic data compatible with oral administration of PF-05190457 but also unexpected (reversible) pharmacological effects, *i.e.* tachycardia and somnolence. While the former can be attributed to a probable peripheral effect, the latter requires further investigation to be linked to the brain impairment of PF-05190457.[32]

In the present publication, we describe the structure-based rational design, synthesis details and pharmacological characterization of a novel GHSR-IA chemotype. The most promising compound **47** shows significant brain exposure and may represent an important step towards therapeutic agents to treat metabolic disorders related to obesity, such as type-2 diabetes mellitus.

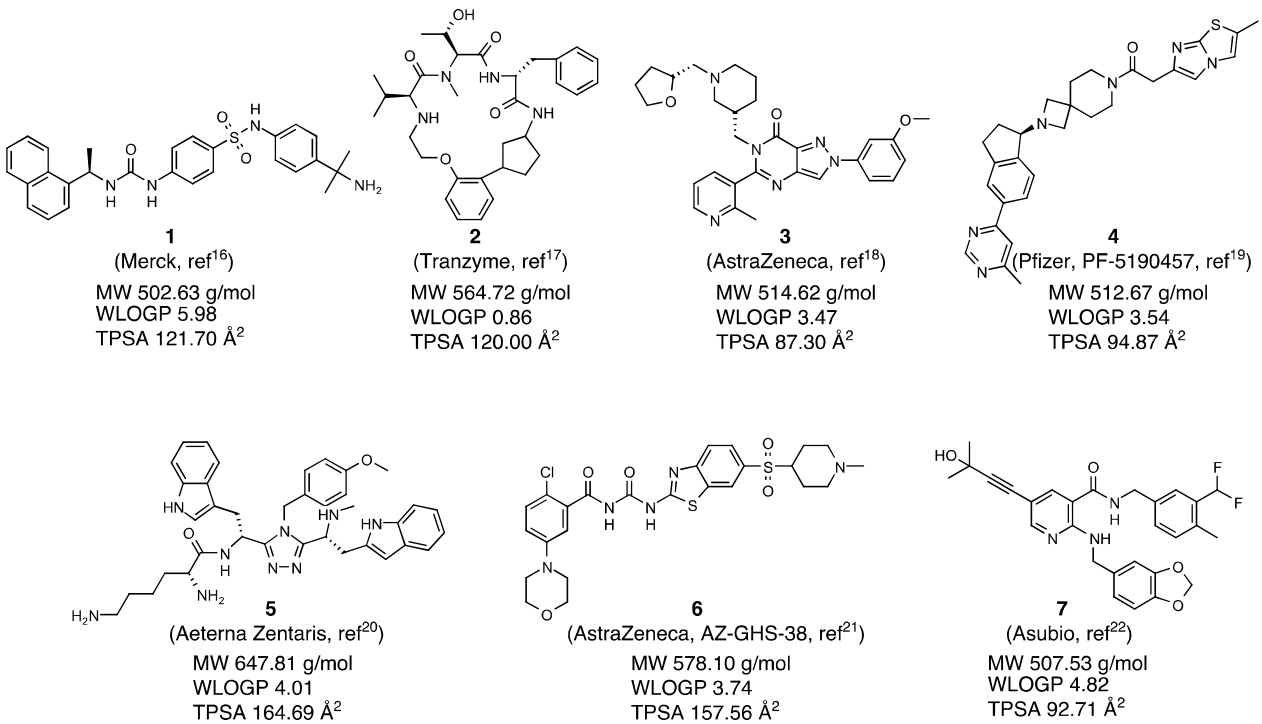

Figure 1. Representative structures of chemical series reported as ghrelin inverse agonists

(GHSR-IA); in brackets are the name of the company, the seminal reference, and when found, an identifier. Parameters calculated with the SwissADME web tool;[24] MW: molecular weight; WLOGP: in-house implementation of Wildman and Crippen log *P*;[33] TPSA: topological surface area.[23]

RESULTS AND DISCUSSION

Our very first step in crafting a novel chemotype able to inversely agonize GHSR was to compare the structure of the most advanced GHSR-IA, *i.e.* compound **4** (PF-05190457, Figure 2)[19] with bioactive modulators of GHSR from Helsinn's proprietary collection.[34] Compound **8** (H0700, Figure 2) was selected based on its potent purely competitive antagonist activity in FLIPR assay and on its favorable properties for absorption, distribution, metabolism and excretion (ADME) and for pharmacokinetic (PK) profile.

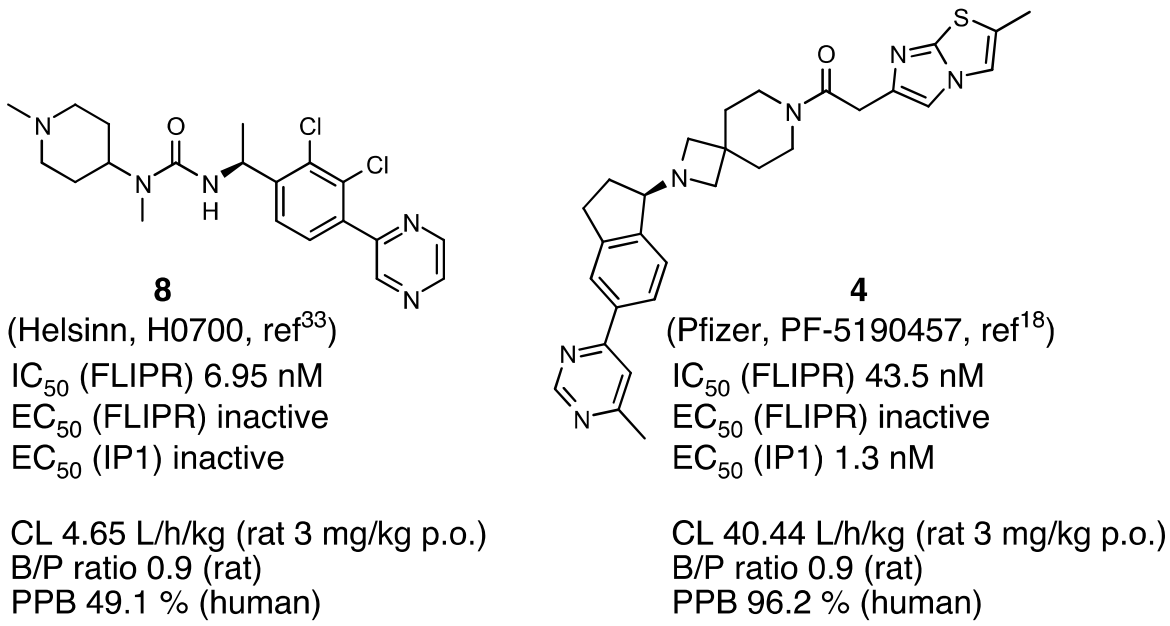

Figure 2. Competitive GHSR antagonist (**8**, H0700) with favorable ADME and PK profile and state-of-the-art GHSR-IA (**4**, PF-5190457) used as template structures for the chimeric design. IC_{50} (FLIPR) measures antagonism, EC_{50} (FLIPR) measures agonism, EC_{50} (inositol phosphate accumulation assay, IP-1) measures inverse agonism. CL is for clearance, B/P ratio for brain/plasm concentration ratio and PPB for plasma protein binding (refer to *Experimental Section* for details).

Generation of structure-based hypothesis. Superimposition of **4** and **8** was achieved by predicting their most probable binding mode in a theoretical tridimensional structure of human GHSR retrieved from the ModBase repository (https://modbase.compbio.ucsf.edu/). *In silico* docking was performed with the Attracting Cavities (AC) method[35], which not only was proven a high-performing and broadly applicable docking engine but also allows for flexibility of the

binding site residues, thus potentially fixing structural uncertainties imputable to homology models. The inner channel of GHSR to study was defined as an extended search volume encompassed in a rectangular parallelepiped of 24 x 20 x 33 Å, with Phe309 side chain as center and the longer side of the box in the main orientation of the receptor (refer the *Experimental Section* for more details).

As depicted in Figure 3A, our computer modeling investigation predicted the acidic residue Glu124 as chief anchor point that drives the recognition of **4** and **8** by GHSR. The salt-bridge counterparts in both ligands are basic nitrogen atoms allowing highly stabilizing ionic interactions. This is in accordance with mutagenesis studies evidencing the critical importance of Glu124 to generate an agonistic response by recognizing ghrelin or other ligands, without impacting the ligand-independent activity of GHSR.[36,37] Furthermore, Glu124 is involved in ionic interactions with a variety of positively charged peptide and non-peptide GHSR modulators.[38,39] This pharmacophoric basic moiety is located differently in compounds **4** and **8**. Indeed, the methylpiperidine is at one end of molecule **8**, whereas the spiroazetidine is central in the structure of **4**. Little rotational adaption of Glu124 side chain is observed upon binding (Figure 3B), making both basic nitrogens not exactly superimposed in the binding site. More drastic conformational changes are required for GHSR to accommodate the large dihydroindene-methylpyrimidine terminal moiety of **4**. An additional cavity is made accessible deeper inside the receptor structure (in translucent pink in Figure 3A) mainly through motions of Trp276, Phe279, Phe312 and Phe309 bulky side chains (refer to Figure 3B). Thanks to these conformational rearrangements, and other more modest geometrical changes, **4** can make favorable interactions with amino acids deeper inside GHSR, either aromatic or hydrogen-bonding. The most

remarkable interactions include the indane moiety in sandwich pi-stacking between Phe279 and Phe312, as well as the methylpyrimidine making aromatic interaction with Trp276, with both nitrogen heteroatoms accepting hydrogen-bond from Thr127 and Ser315, respectively. Phe279, Phe312 and Phe309 are part of the *aromatic cluster*, which was described by Holst *et al.*[40] as an important motif for the binding of (agonists or antagonists) substance-P analogues on GHSR.[41] Further supporting our predictive computer model, the opening of the deeper additional cavity is reported as possible binding mode of carboxyamidated wFwLL peptides.[42] This study strongly suggests that ligands binding deep in the GHSR cavity show inverse agonist effect by preventing the motion of extracellular part of two transmembrane domains (TM-VI and VII, bearing the *aromatic cluster*), which is mandatory for activation. On the contrary, agonistic ligands are expected to show a superficial binding mode. The chemical series from which H0700 (molecule **8**) belongs comprises many GHSR agonists with very similar chemical structure.[43] It is thus inferred that compounds of this chemotype have very similar binding modes, regardless being agonist or antagonist.

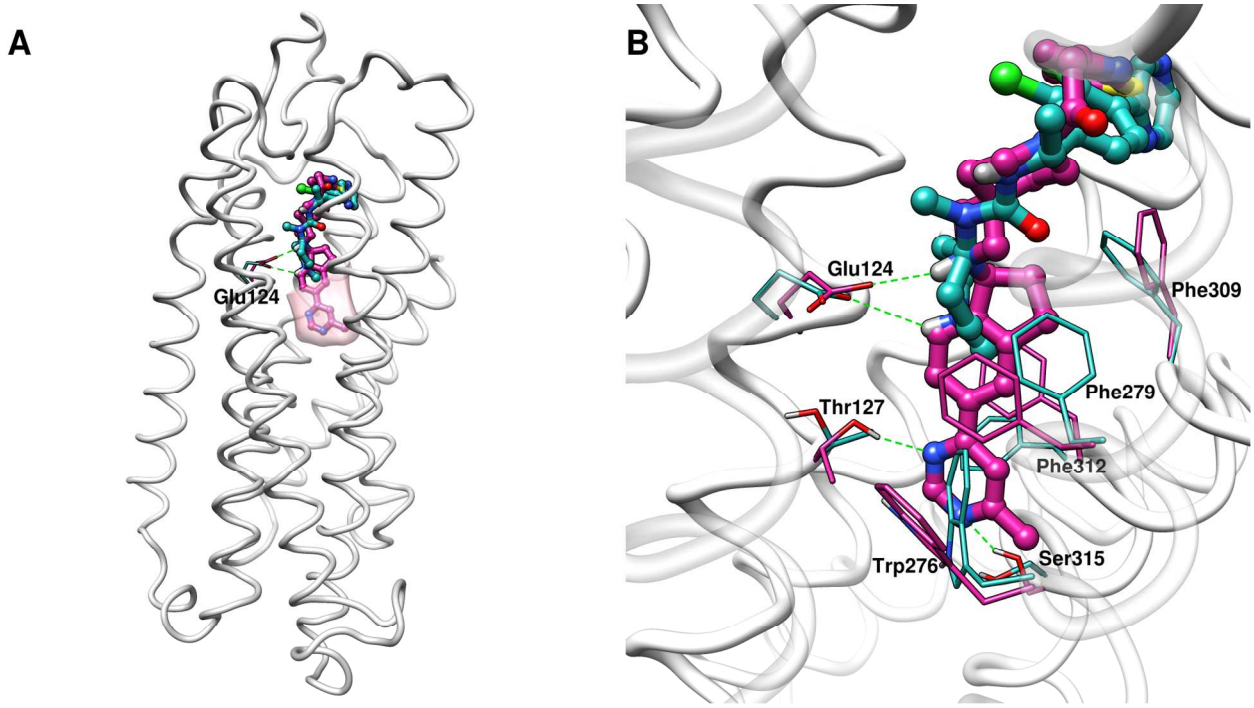

Figure 3. Predicted binding modes of compounds **4** (inverse agonist, PF-05190457, carbon atoms in magenta) and **8** (antagonist, H0700, carbon atom in turquoise) in GHSR (white cartoon, extracellular compartment on the top). Non-polar hydrogens are hidden for clarity. (A) General view with the major anchor point Glu124 making ionic interactions (dashed green lines) with the basic nitrogen of each molecule. An additional deeper cavity (in translucent pink) is accessible to accommodate the large dihydroindene-methylpyrimidine terminal moiety of **4**. (B) Zoom into the binding site showing significant motions of key residues upon docking of **4**, which open the deeper cavity and/or make additional intermolecular interactions (polar in dashed green lines, or aromatic). Carbon atoms of the ligand (balls-and-sticks) and of the residues (thin sticks) are of the same color for a given calculated binding mode.

.

Three families of chimeric compounds. The robust structural hypothesis generated by the *in situ* superimposition of a central GHSR antagonist (**8**) with a peripheral GHSR-IA (**4**) enabled

the design of chimeric molecules. Our aim is the discovery a novel GHSR modulator chemotype displaying different pharmacokinetic and pharmacodynamic properties compared to the state-of-the-art.

Three families of chimeric structures were designed as depicted in Figure 4 and evaluated for their GHSR-IA potential. The "spiro" molecules (**9** and **10** in Table 1) were designed by merging the whole left-hand 2-[5-(6-methylpyrimidin-4-yl)-2,3-dihydro-1H-inden-1-yl]-2,7-diazaspiro[3.5]nonane-7-carbaldehyde part from **4** with the urea function of **8**; the "piperidine" molecules (**11** and **12** in Table 1) are resulting from connecting the left-hand 4-(2,3-dihydro-1H-inden-5-yl)-6-methylpyrimidine end from **4** directly on the piperidine of **8**; and the "imidazothiazol" (**13** and **14** in Table 1, for challenging the "inverse-agonist-deeper-binding" hypothesis) simply replaces the right-hand aromatic rings of **8** by the methylimidazothiazol system of **4**.

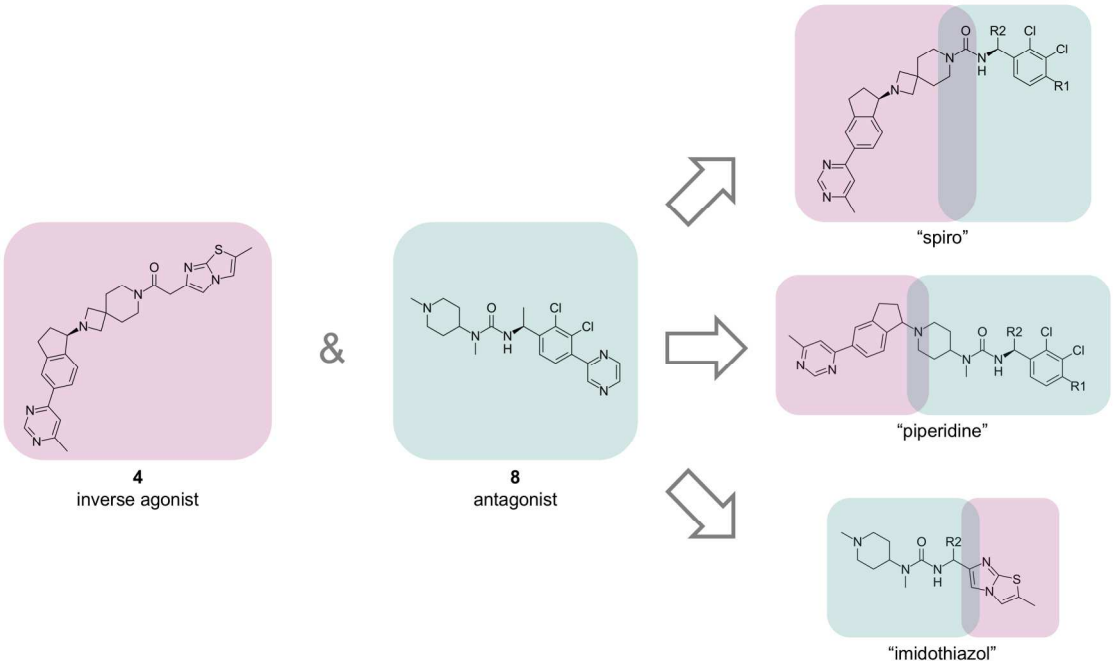

Figure 4. Chimeric design from template molecules **4** and **8** to generate "spiro", "piperidine" and "imidothiazol" families of structures. The parts of the crossover structures are boxed in colors corresponding to the molecule they are originated from (pink for the inverse agonist and turquoise for the antagonist; grey is for overlay regions).

Table 1. Evaluation of three families of chimeric molecules as GHSR modulators

Cmpd	family[a]	R1[a]	R2[a]	FLIPR EC_{50} (nM) agonism	FLIPR IC_{50} (nM)[c,d] antagonism	IP-1 EC_{50} (nM)[c,d] inverse agonism
9	spiro		Me	> 30000	1210	483
10	spiro	H	Me	> 30000	4010	inactive
11	piperidine		Me	> 30000	369	194
12	piperidine	H	Me	> 30000	2330	inactive
13	imidazothiazol	n/a[b]	Me	> 30000	> 30000	inactive
14	imidazothiazol	n/a	H	> 30000	> 30000	inactive

[a]refer to Figure 4; [b]not applicable; [c]mean of at least two independent measurements done in triplicates; [d]SEM was less than 25% for all values.

None of the molecules tested in FLIPR assay (**9**-**14**) displayed agonistic activity. Both compounds belonging to the "imidazothiazol" family (**13** and **14**) were found inactive in all three FLIPR and IP-1 assays. This result verifies an early SAR observation made from Helsinn's asymmetric urea scaffold, which suggested that GHSR modulation requires a benzylic moiety on the right-hand side of the ligand structure.[33,43] Accordingly, all molecules of the "spiro" (**9** and **10**) and of the "piperidine" (**11** and **12**) families were found bioactive on the GHSR. In both families, the pyrazine substitution in R1 increased antagonism potency in FLIPR by a factor of 3

and 6 for the "spiro" and "piperidine" compounds, respectively. Nevertheless, unsubstituted compounds in R1, **10** and **12**, retained weak GHSR antagonistic activity with IC_{50} of 4.0 μM and 2.3 μM, respectively. This is in agreement with previous SAR.[34] Most gratifyingly, the pyrazine substituted compounds displayed sub-micromolar GHSR inverse agonism activity in IP-1 assay, with EC_{50} of 483 nM and 194 nM for **9** and **11** respectively. Because both "piperidine" compounds showed higher potency, this family of chimeric structures was selected as a molecular scaffold for further optimization. Chemical variations were first undertaken on the *p*-substitution of the dichlorobenzyl right-hand part (R1 in Tables 1 and 2).

Table 2. Exploration of right-hand dichlorobenzyl *p*-substitution of the "piperidine" scaffold: potency and metabolic stability.

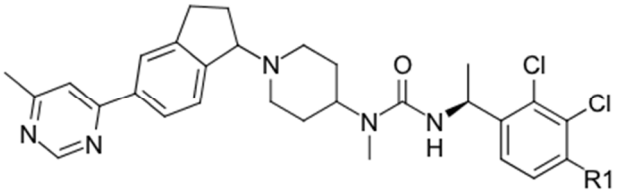

Cmpd	R1	FLIPR IC_{50} (nM)[b,c] antagonism	IP-1 EC_{50} (nM)[b,c] inverse agonism	Clearance human microsome (μL/min/mg)	Clearance mouse microsome (μL/min/mg)	Clearance rat microsome (μL/min/mg)	Clearance dog microsome (μL/min/mg)
11		369	194	n/d[a]	n/d	n/d	n/d
15	OMe	171	67	94.2	122	69.5	241.1
16	COOMe	303	96	n/d	n/d	n/d	n/d
17	COOH	> 30000	inactive	n/d	n/d	n/d	n/d
18	NH_2	571	121	n/d	n/d	n/d	n/d

19	ethynyl	156	10.6	165.1	157.2	65.6	136.9
20	cyclopropyl	2870	298	n/d	n/d	n/d	n/d
21	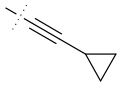	80	51	53.9	42.6	19.2	62.3

[a]not determined; [b]mean of at least two independent measurements done in triplicate; [c]SEM was less than 25% for all values.

Chemical explorations on the "piperidine" family. Table 2 shows the potency and (for selected ones) the metabolic stability of compounds featuring eight different *p*-substituents of the dichlorophenyl moiety instead of the pyrazine as in **11**. The only fully inactive molecule was the benzoic acid derivative (**17**), whereas its methylbenzoate analog (**16**) showed increased potency in both antagonism and inverse agonism assays compared to **11**. This indicates that a negative charge at that position is not tolerated, contrarily to a polar group. A decrease of activity on GHSR compared to **11** is observed for the cyclopropyl substituted molecule (**20**), mainly in FLIPR, but also in IP-1. The aniline analog (**18**) turned out to be a slightly more potent inverse agonist, but with less antagonistic behavior than **11**. The most significant increases of inverse agonism activity were measured for the dichlorobenzyl *p*-methoxy (**15**) *p*-ethynylcyclopropane (**21**) and *p*-ethynyl analogues (**19**). As a first evaluation for metabolic stability of the latter three molecules, clearance was measured in liver microsomes from different sources (human, mouse, rat and dog). Remarkably, the most hydrophobic ethynylcyclopropane substituent led to molecule **21**, which is clearly more stable in all four species compared to **15** and **19**. This is fundamental for further preclinical evaluations and offers good prospects for BBB permeation ability, with the aim of obtaining a centrally acting GHSR-IA. Besides, **21** showed a potent GHSR antagonism in FLIPR assay. According to these initial results, compound **21** represents

already an interesting candidate to be promoted for further preclinical investigation. However, for the sake of possible physicochemical optimization towards drug-likeness, further modifications on the "piperidine" family were performed to broaden the chemical space explored.

Table 3 shows the exploration on the benzylic position at the right-hand side of the "piperidine" scaffold (R2) together with some variations on the *p*-substituents of the dichlorobenzyl (R1), based on previous results (as in Tables 2).

Table 3. Exploration of right-hand benzylic position of the "piperidine" family.

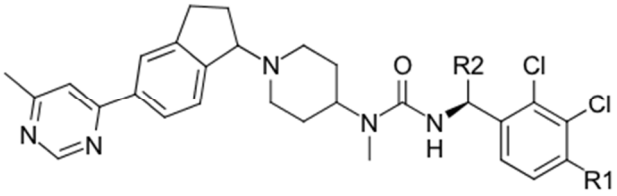

Cmpd	R1	R2	FLIPR IC_{50} (nM)[a,b] antagonism	IP-1 EC_{50} (nM)[a,b] inverse agonism
22	H	H	2700	inactive
23	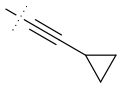	H	1130	inactive
24	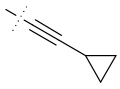	ethyl	192	306
25		CF_3	8080	2164

26			4540	484
27	H		5400	970
28	OMe		1800	439

[a]mean of at least two independent measurements done in triplicates; [b]SEM was less than 25% for all values.

An unsubstituted benzyl position (R2) annihilates inverse agonism of "piperidine" molecules with the dichlorobenzyl para position (R1) substituted (**23**) or not (**22**). Also, comparison with methylated counterparts (**21** et **12**, respectively) shows that the antagonism effect of **23** and **22** is lower. Following previous SAR, we selected a small set of well-tolerated alkyl substituents that retained antagonism when placed in the benzylic position in a previous series.[34] Replacing methyl (**21**) by ethyl (**24**) at the benzylic position decreased the inverse agonism potency 6-fold and the antagonism potency 2.5-fold. The decrease was even more important when trifluoromethyl or a bulky group such as cyclopropylmethylene is at the benzylic position (see **25**, **26** compared to **11**, and **28** compared to **15**). As a consequence, in this chemical context, a methylated benzylic position appears optimal for GHSR modulation and thus no further explorations nor analyses regarding this position were pursued.

Attention was then given to the left-hand side of the "piperidine" chimeric structures. Table 4 shows the SAR of fourteen derivatives focusing on the left-hand indane substitution in position 5 (R3) together with some variations on the *p*-substituents of the right-hand dichlorobenzyl (R1), based on previous results (as in Tables 2 and 3).

Table 4. Exploration of left-hand indane substitution in position 5 of the "piperidine" scaffold: potency and metabolic stability.

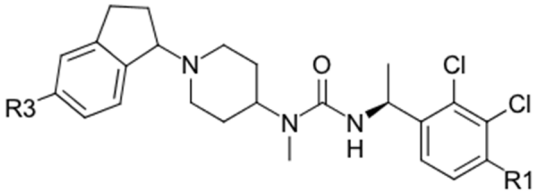

Cmpd	R1	R3	FLIPR IC_{50} (nM) [b,c] antagonism	IP-1 EC_{50} (nM) [b,c] inverse agonism	Clearance human microsome (µL/min/mg)	Clearance mouse microsome (µL/min/mg)	Clearance rat microsome (µL/min/mg)	Clearance dog microsome (µL/min/mg)
29	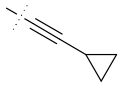		798	634	n/d[a]	n/d	n/d	n/d
30	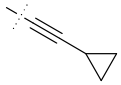		85.9	84.8	n/d	n/d	n/d	n/d
31	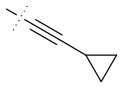	Me	282	117	n/d	n/d	n/d	n/d
32	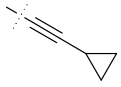	H	919	inactive	n/d	n/d	n/d	n/d
33	OMe	Me	329	73	80.3	216.8	143.1	168.5
34	OMe	Cl	315	40.7	241.2	387.5	270.8	n/d
35	OMe	OMe	120	85.7	n/d	n/d	n/d	n/d
36	OMe	OH	1300	inactive	87.1	117.3	n/d	n/d
37	OMe	NH_2	1510	inactive	47.1	70.4	n/d	n/d
38	OMe		240	70	79.8	244	n/d	n/d

39	OH	Me	1166	189	n/d	nd	n/d	n/d
40	etynyl	Me	106	inactive	n/d	n/d	n/d	n/d
41	cyclopropyl	Me	2367	inactive	n/d	n/d	n/d	n/d
42	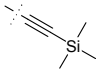	Me	2005	inactive	n/d	n/d	n/d	n/d

[a]not determined ; [b]mean of at least two independent measurements done in triplicates; [c]SEM was less than 25% for all values.

Exchanging 6-methylpyrimidine (**21** in Table 2) in position 5 of the dihydroindene by pyrimidine reduced the antagonism and the inverse agonism effects to very different extent with respect to isomers (refer to **29** and **30** in Table 4). This indicates the sensitivity of this pharmacophoric zone, in agreement with the localized hydrogen-bonding interactions involving both azaheteroatoms of **4** with Thr127 and Ser315 in the deeper cavity of GHSR and hypothesized related to inverse agonism (refer to Figure 1B).

Whereas a non-substituted dihydroindene at position 5 annihilates inverse agonism (**32**), a methyl substitution (**31**) leaves some hope of significantly reducing the size of the molecule (potentially more druglike and BBB permeant) yet keeping the inverse agonistic capability. This was partly achieved by **33**, bearing a para-methoxy on the dichlorophenyl (EC_{50} of 73 nM in IP-1). However, **33** was unstable in liver microsomes, especially in rodents and dog, which could hamper further development. Unfortunately, other 5-methyldihydroindene analogues with variation in para of dichlorophenyl did not show inverse agonism activity on GHSR (**39**, **40**, **41**, **42**). All other attempts of including diverse small substituents in position 5 of the dihydroindene

while keeping *p*-methoxydichlorophenyl on the right-hand side failed at producing metabolically stable and potent GHSR-IA (**34**, **35**, **36**, **37**, **38**).

Finally, Table 5 lists the result of a very limited number of variations on the central "piperidine" based on the experience gained in asymmetric urea GHSR effectors[33,43]. Compound **21** was modified by applying changes able to retain agonistic or antagonistic activity in previous series.

Table 5. Chemical variation on the central "piperidine" core.

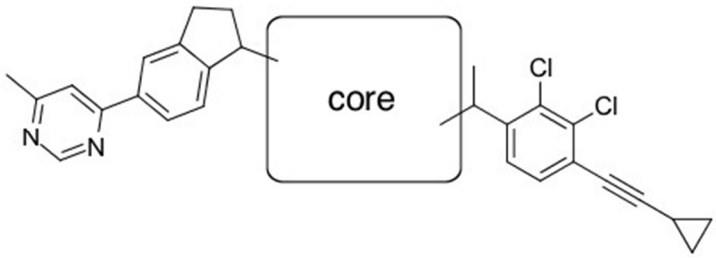

Cmpd	core	FLIPR IC50 (nM)[a,b] antagonism	IP-1 EC_{50} (nM)[a,b] inverse agonism
43	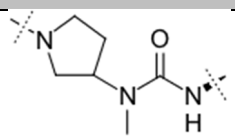	148	inactive
44	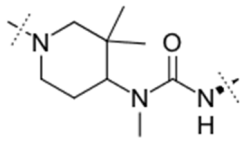	530	363
45	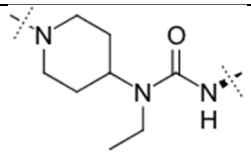	2920	937

[a]mean of at least two independent measurements done in triplicates; [b]SEM was less than 25% for all values.

While the pyrrolidine compound (**43**) did not show inverse agonism activity, other two piperidine molecules (**44**, **45**) confirmed the GHSR inverse agonism ability of this chemotype, with antagonism effect as well. However, these changes on the piperidine core (i.e. gem-dimethyl **44** and ethyl urea **45**) did not improve the potency, failing to decrease IC_{50}/EC_{50} below 100 nM neither in FLIPR nor IP-1 assays. Consequently, they were not considered for further exploration.

As a result of the presented SAR investigations, one of the first examples of the promising new "piperidine" scaffold, i.e. the diastereomeric mixture **21,** showed the best potential for further investigation. Chiral HPLC enabled separation at the asymmetric center on the indane moiety of **21** (the benzylic asymmetric carbon is kept in *S* as a known determinant for GHSR activity in all tested asymmetric urea series)[34,44]. As shown in Table 6, a drastic drop of antagonist and inverse agonist potency can be observed for the *S*-enantiomer (**46**), whereas the *R*-enantiomer (**47**) show an increase of activity in FLIPR and more significantly in IP-1, compared to **21**.

Table 6. Exploration of compound 21 chirality.

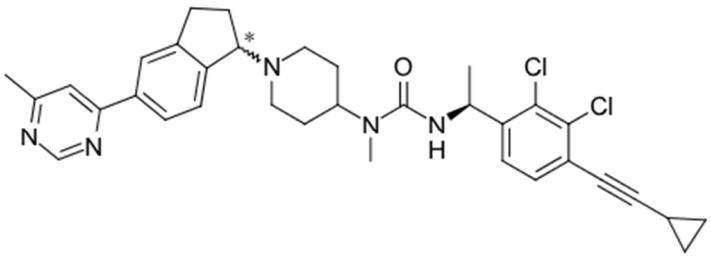

Cmpd	Chirality of *	FLIPR IC50 (nM)[b,c] antagonis	IP-1 EC50 (nM)[b,c] inverse agonism	Clearance human microsomes (µL/min/mg)	Clearance mouse microsomes (µL/min/mg)	Clearance rat microsomes (µL/min/mg)	Clearance dog microsomes (µL/min/mg)

		m					
21	racemate	80	51	53.9	42.6	19.2	62.3
46	*S*	1276	1276	n/d[a]	n/d	n/d	n/d
47	*R*	68.2	29.4	74.7	<10	57.8	52.2

[a]not determined ; [b]mean of at least two independent measurements done in triplicates; [c]SEM was less than 25% for all values.

Interestingly, the differences in *in vitro* metabolic stability for compounds **47** and **21** depended very much on the species. Whereas the clearance in human and rat microsomes was higher for **47**, the clearance in dog microsomes was measured lower. The most significant variation is seen in mouse liver microsomes where **47** was very stable. This latter result is of crucial importance for preclinical assessments in this species. Therefore, the most active stereoisomer of the most promising compound (i.e. compound **47**) was promoted for further evaluation as a GHSR-IA potential preclinical candidate.

Pharmacodynamics and binding mode of 47. Molecule **47** (structure in Figure 5A) reached high level of GHSR inverse agonism in IP-1 assay (EC_{50} = 29.4 nM) as well as antagonism in FLIPR test (IC_{50} = 68.2 nM). The binding mode of **47** in GHSR was predicted through molecular docking following the exact same protocol as for the template molecules **4** and **8**. Figure 5B shows how inverse agonist **47** is suitably accommodated deep inside the GHSR cavity. Similarly to modeled Pfizer's molecules **4**, residues Phe279, Phe312 and Phe309 moved in order to open the deeper side pocket and to make aromatic interactions with the ligand. In the case of **47**, an extra aromatic interaction with Phe221 is predicted. Besides, the most favorable positioning shows a rotated 4-methylpyrimidine ring compared to **4.** This favors a distinct hydrogen-bonding network involving both azaheteroatoms with Thr130 and Trp276, whereas the methyl substituent

makes purely Lennard-Jones contacts with the backbone of TM2. Other hydrophobic interactions can be observed with the side chains of Cys126 and Ile92. Apart from the chief anchoring salt-bridge between the basic nitrogen and Glu124, the piperidine moiety is in contact with Gln120 and Arg283 side chains. The latter are two important residues for GHSR intrinsic activity, and for the binding of agonistic and inverse agonistic ligands as well.[42] As described for the binding of various ghrelin receptor agonists,[37] the arginine is predicted to make not very specific intermolecular interactions, but an extended part of **47** urea-piperidine central core is "leaned" on the side chain. This extended contact area by itself may explain the importance of Arg283 for the binding of such molecular structures. Gln120 is predicted to point towards both chlorine atoms, which may indicate some electronic interplay in that region of the binding site. The dichlorophenyl ring is principally involved in a cation-pi interaction with the guanidine of Arg199, which was found as an essential residue for the effect of pioneer growth hormone secretagogue L-692,429, for instance.[3,45] Another important amino acid for ligand binding, Phe286,[37] is predicted in aromatic interaction with dichlorophenyl moiety. The *p*-ethynylcyclopropane substituent is in hydrophobic contacts with Arg102 and Leu103. The cyclopropane ring can be part of more specific interactions with Tyr106 side chain, possibly with the aromatic and/or as a weak hydrogen-bond acceptor.

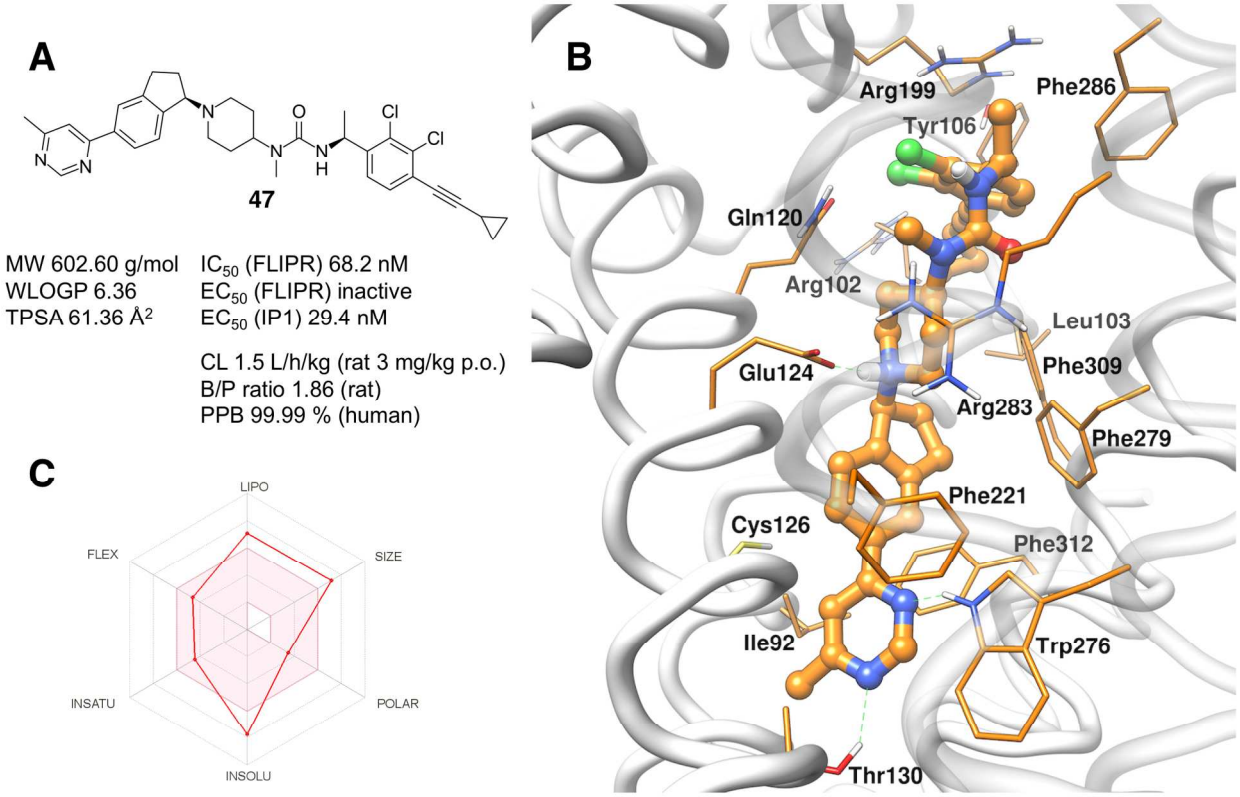

Figure 5. Potential preclinical candidate GHSR-IA, compound **47**. (A) Chemical structure and parameters (physicochemical, PD and PK). (B) Predicted binding modes (balls-and-sticks) in GHSR (white cartoon, and interacting residues in thin sticks). All carbon atoms are in orange, while non-polar hydrogens are hidden for clarity. The model shows how **47** is salt-bridged to Glu124 (dashed green line) and how it interacts specifically with residues deep in the cavity, *e.g.* accepting hydrogen-bond from Thr130 and Trp276 (dashed green lines) or making aromatic interactions with Phe221, Phe279, Phe309 and Phe312. Other important interactions to rationalize binding include Arg199, Arg283 and Phe286. Finally, the ligand is in contact with Ile92, Arg102, Leu103 Gly120 and Cys126. (C) The Bioavailability Radar generated with SwissADME[24] shows suitable polarity, flexibility and saturation for **47** but suboptimal lipophilicity, size and solubility, which can explain moderate oral bioavailability in rat (F = 27.2%).

ADME and pharmacokinetic parameters of 47. Molecule **47** was found metabolically stable *in vitro* showing a very low intrinsic clearance in mouse liver microsomes. In microsomes from other species (human, rat and dog), the intrinsic clearance was higher, albeit inferior compared to the less lipophilic compounds of the same structural class (for racemate **21** vs. **15** and **19**, refer to Table 2). Despite the relative liability *in vitro* in rat liver microsomes, compound **47**, after intravenous administration to rat (3 mg/kg), showed low plasma clearance (0.91 L/h/kg), long half-life ($t_{1/2}$ = 6.49 h), large volume of distribution (V_d = 8.48 L/kg) and remarkable brain penetration with a brain/plasma (B/P) ratio of 1.86 (at 2h). After oral administration (3 mg/kg), compound **47** showed moderate bioavailability (F = 27%), a long absorption phase (T_{max} = 6.7 h) and longer half-life ($t_{1/2}$ = 15.85 h) than after intravenous administration.

The main parameter affecting bioavailability of **47** is certainly the poor permeability as determined in Madin-Darby Canine kidney cells expressing multidrug resistance protein 1 (MDR1-MDCK). Apparent permeability of **47** (when inhibiting MDR1 with ciclosporine) was measured as low as $P_{A\rightarrow B} = 2.4x10^{-6}$ cm/s. The Bioavailability Radar of molecule **47** generated through the SwissADME Web tool[24] and plotted in Figure 5C indicates size (602.60 g/mol), high lipophilicity (WLOGP = 6.36) and poor solubility (predicted[46] log *S* = -7.75) as the main properties responsible for the moderate oral bioavailability. Unfortunately, all attempts made to correct these suboptimal properties failed at producing "piperidine" core molecules with potent GHSR inverse agonistic activity. Moreover, **47** was determined highly bound to plasma protein (99.99% in human, rat and dog and 99.98% in mouse). However, a big and lipophilic molecule like **47** was found metabolically stable *in vivo* and notably in significant CNS concentration in rat's brain probably thanks to its moderate apparent polarity (TPSA 61.36 $Å^2$) although active transport into the brain cannot be excluded. Finally, **47** was predicted (by SwissADME[24]) and

afterward experimentally confirmed in MDR1-MDCK cells not to be a substrate of the P-gp efflux pump ($P_{A\rightarrow B}$ = 3.9x10^{-6} cm/s, when MDR1 not inhibited). These results rewarded our effort in designing a central GHSR-IA and thus compound **47** entered first assessments for reduction of food intake in rodents.

Pharmacological characterization of 47. Preliminary *in vivo* efficacy was encouraging. A first experiment was designed to evaluate the ghrelin inverse agonist activity on an animal model. To this aim, we have measured the ability of molecule **47** to counteract the increase of food intake induced by a ghrelin agonist, i.e. anamorelin. Anamorelin was used as a reference standard GHSR agonist compound, for which the ability to increase food intake and body weight has been well characterized in rodent models, as well as in human.[47] Fed mice were given **47** either 10 mg/kg i.p. (n=6) or 30 mg/kg p.o. (n=6), and 10 min later, anamorelin 30 mg/kg p.o. The total amount of food intake measured at 1, 2, 4, 8 and 24 h. after dosing are shown in Table 7.

Table 7. Increase of food intake in mice counterbalanced by compound 47.

T [a] (h)	VEH [b]	VEH+ANA [c]	VEH+ANA+Cmpd **47** (10 mg/kg i.p.)	VEH+ANA+Cmpd **47** (30 mg/kg p.o.)
1	0.24 ± 0.02	0.63 ± 0.04	0.13 ± 0.02*	0.22 ± 0.02*
2	0.45 ± 0.03	1.37 ± 0.05	0.56 ± 0.03*	0.86 ± 0.20
4	0.79 ± 0.02	2.09 ± 0.08	1.66 ± 0.08	1.45 ± 0.15
8	1.38 ± 0.05	2.97 ± 0.09	2.78 ± 0.05	1.80 ± 0.08*
24	7.23 ± 0.3	8.31 ± 0.2	7.63 ± 0.8	7.42 ± 0.5

Cumulative food intake (in g) as the mean values ± SEM (n=6); [a]time after administration;[b]VEH: vehicle; [c]ANA: anamorelin (30 mg/kg p.o.); *p<0.05 *vs*. VEH+ANA (ANOVA plus Dunnett t test)

Compound **47** inhibited food intake, induced by anamorelin, by 38.2% at 8 h. after 10 mg/kg intraperitoneal administration with activity observed up to 8 hours. Moreover, inhibition of food intake reached 78.2% at 1 hour after 30 mg/kg oral administration with activity observed up to 2 hours. Although interspecies translation regarding the brain penetration of compound **47** cannot be proven at this stage, these *in vivo* results represent an additional strong indication of this chemotype potential for central action on obesity-related metabolic disease. Additional preclinical evaluation experiments are required for confirmation.

Furthermore, *in vitro* inhibition of hERG was measured at IC_{50}=3.16 μM. Whereas this preliminary evaluation should not be considered as a severe warning, cardiovascular safety issues cannot be ruled out. Further experimental assessments on off-target activities are necessary at later preclinical stage, first *in vitro* on other ion channels and generally on a diverse panel of biotargets. Final evaluation will require *in vivo* monitoring of cardiovascular parameters in different animal species, when the dose can be anticipated.

SAR, optimization of physicochemical properties and initial *in vivo* data allowed to identify **47** as a suitable candidate for further preclinical investigations as centrally acting GHSR-IA.

Synthesis. Chemical syntheses of various intermediates and the corresponding derivatives are depicted in Schemes 1-8. Heterocyclic substituted 2,3-dihydro-1H-inden-1-ones were synthesized starting from 5-bromo-2,3-dihydro-1H-inden-1-one by Suzuki coupling[48] (**9-6**, **29-1**, **30-1)** or Buchwald amination[2] (**38-1**) (refer to Scheme 1). *tert*-Butyl (1-oxo-2,3-dihydro-1H-inden-5-yl)carbamate (**37-5**) was prepared by CO insertion reaction followed by hydrolysis and Curtis rearrangement with DPPA/*t*-BuOH[49].

Scheme 1. Synthesis of substituted 2,3-dihydro-1H-inden-1-one derivatives

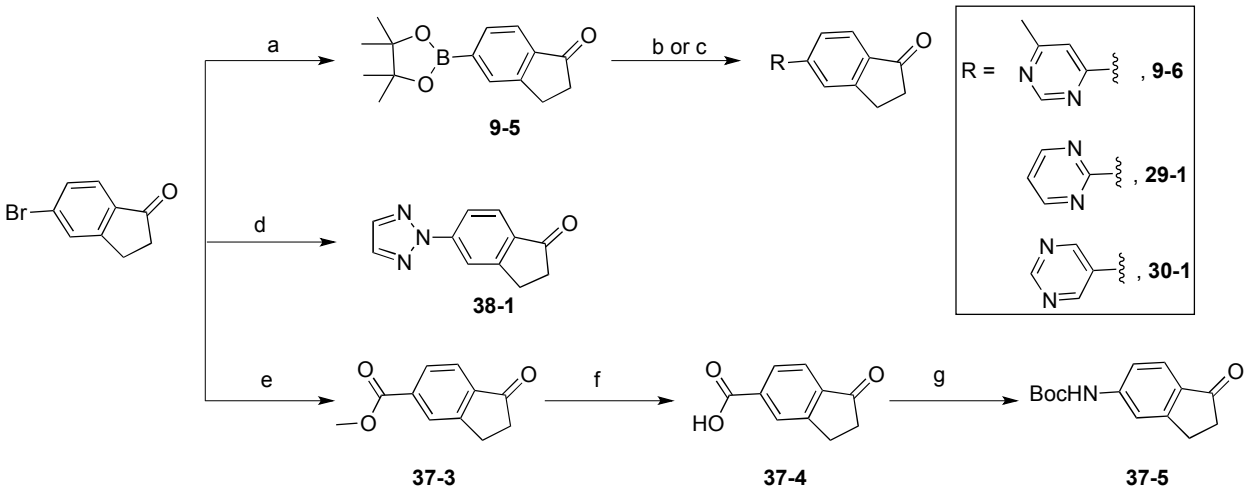

Reagents and conditions: (a) $Pd(PPh_3)Cl_2$, 4,4,4',4',5,5,5',5'-octamethyl-2,2'-bi(1,3,2-dioxaborolane), KOAc, dioxane, 29%; (b) $Pd(PPh_3)_4$, 4-chloro-6-methylpyrimidine or 5-bromopyrimidine, Na_2CO_3, dioxane/H_2O, reflux, overnight, 64% for **9-5** and 47.6% for **30-1**; (c) $Pd(dppf)Cl_2$, Na_2CO_3, DME, 95°C, overnight, 41% for **29-1**; (d) triazole, $Fe(acac)_3$, CuO, K_2CO_3, DMF, 80oC, overnight, 21%; (e) $Pd(dppf)_2Cl_2$, CO, TEA, MeOH/DMF, 80°C, overnight, 92%; (f) $LiOH.H_2O$, MeOH/H_2O, rt, 5h, 89%; (g) DPPA/TEA, *t*-BuOH, 90°C, overnight, 32%.

As shown in Scheme 2, intermediates of substituted N-methyl-piperidin-4-amine derivatives (**15-4**, **33-2**, **34-3**, **36-2**) were prepared by reductive amination of 2,3-dihydro-1H-inden-1-ones with benzyl methyl(piperidin-4-yl)carbamate (**15-2**) followed by removal of Cbz group with TMSI[50]. The hydroxyl substituted intermediate (**36-3**) was prepared from demethylation of methoxy substituted intermediate (**36-2**) in the presence of BBr_3 and DCM.

Scheme 2. Synthesis of substituted N-methyl-piperidin-4-amine derivatives

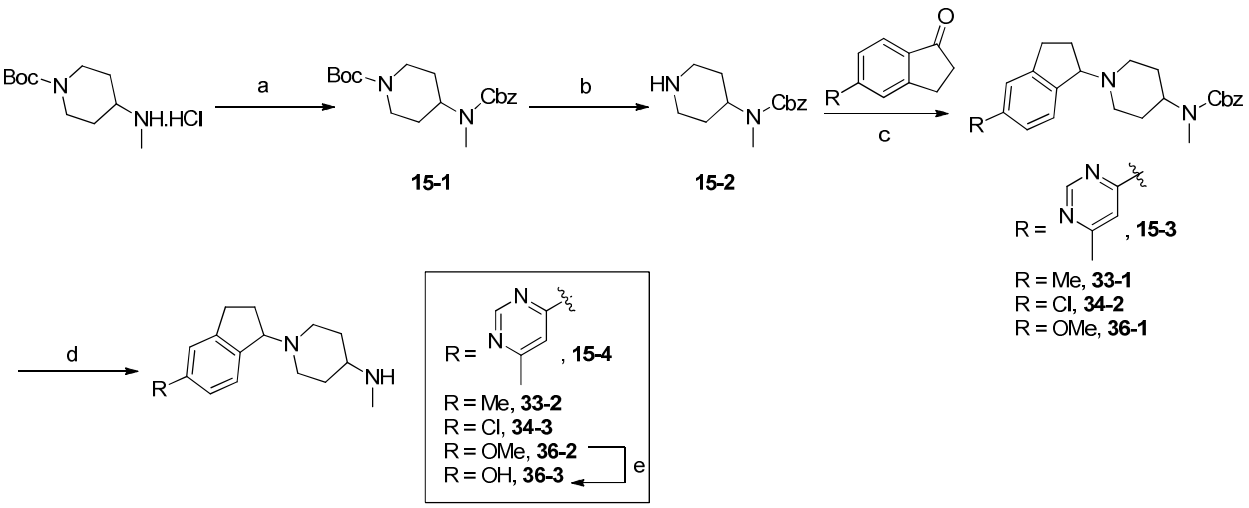

Reagents and conditions: (a) CbzCl, Na_2CO_3 aq., THF, rt, 3h, 80%; (b) TFA/DCM, 0°C, 3h, 100% or MeOH/HCl, rt, overnight, 72%; (c)Ti(i-OPr)$_4$, THF, reflux, 5h~overnight, then $NaBH_3CN$, 50°C, 2h~overnight, 50~78%; (d) TMSI/DCM, 0°C, 1~2h, 57-79%; (e) BBr_3/DCM, 0°C, overnight, 42%

Starting from the iodide **8-1**, several substituted benzylic amines were prepared by Stille coupling (**9-4**), Suzuki coupling (**20-2**) or Sonogashira coupling (**21-2**) followed by removal of Boc group in the presence of acidic conditions (as in Scheme 3). The methoxy substituted benzylic amine (**15-9**) was obtained by chiral separation of the corresponding racemate (**15-8**), which was prepared from 2,3-dichlorophenol in three steps[44].

Scheme 3. Synthesis of substituted benzylic amine derivatives

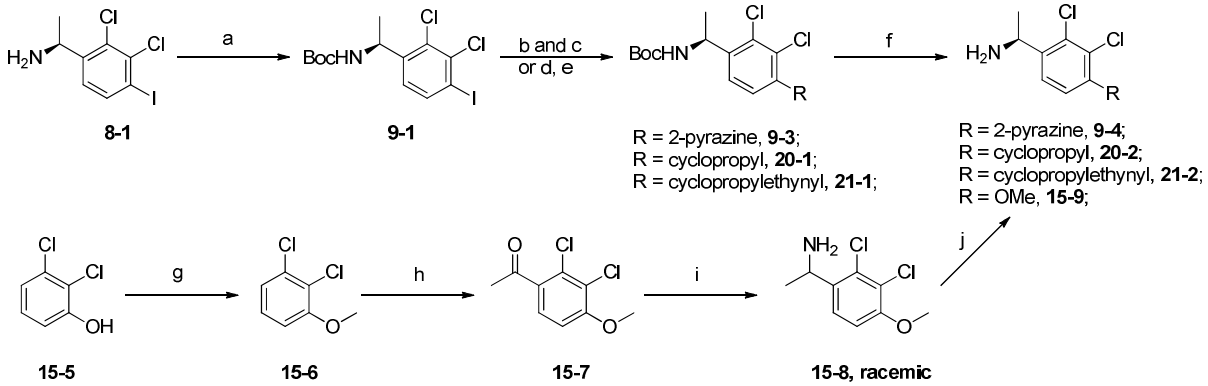

Reagents and conditions:(a) Boc_2O, Na_2CO_3 aq, THF, rt, 2h, 45%; (b) $Pd(PPh_3)_4$, hexamethyldistannane, (n-Bu)$_4$NI, toluene, reflux, 4h, 43%; (c) $Pd(PPh_3)_4$, 2-iodopyrazine, CuI, DME, 110°C, overnight, 36%; (d) cyclopropylboronic acid, $Pd(PPh_3)_4$, Na_2CO_3, Tol/H_2O, 125°C, overnight, 88%;(e) ethynylcyclopropane, $Pd(PPh_3)_2Cl_2$, CuI, TEA, THF, 80°C, overnight, 65%; (f) HCl/dioxane, rt, quantitatively for **9-4** or TFA/DCM, 0°C, 86-95%;(g) DBU, DCM/toluene, reflux, overnight, 94.7%; (h) AcCl, $AlCl_3$, DCM, 10-15°C, 2h, 60%; (i) (1) $HCONH_2$, HCO_2H, 160-170°C, 3h; (2) conc. HCl,reflux, overnight; (j) resolution by chiral HPLC;

The synthesis of spiro analogues (**9** and **10**) is outlined in Scheme 4. First, intermediate **9-8** was prepared by reductive amination of *tert*-butyl 2,7-diazaspiro[3.5]nonane-7-carboxylate with the ketone (**9-6**) according to a slight modification of a procedure reported in the literature [48]. Then the *R*-enantiomer (**9-8A**) was separated by chiral HPLC followed by deprotection and reaction with substituted benzylic amines in the presence of CDI to give the corresponding spiro derivatives (**9** and **10**).

Scheme 4. Synthesis of "Spiro" Family Analogues

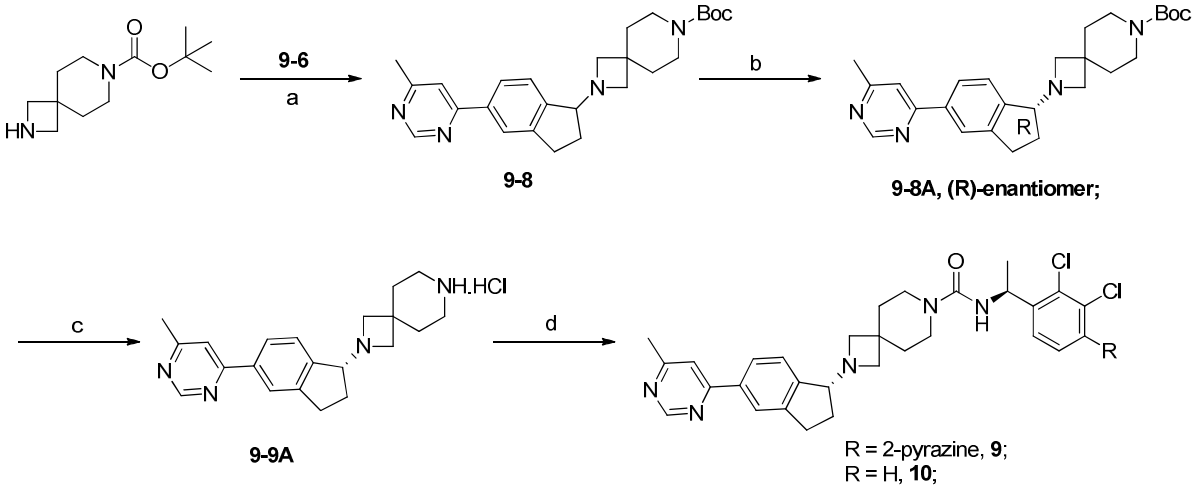

Reagents and conditions: (a) $NaBH_3CN$, NaOAc, MeOH, 0°C~rt, 2 days, 46%; (b) chiral HPLC, ~1/1 of two isomers separated; (c) 4M HCl/dioxane, MeOH, rt, 100%; (d) **9-4** or (*S*)-1-(2,3-dichlorophenyl)ethanamine, CDI/TEA/DCM, 35°C, 37% for **9** and 24% for **10**.

The synthesis of imidothiazole derivatives (**13** and **14**) is outlined in Scheme 5. Starting from 5-methylthiazol-2-amine and ethyl 4-bromo-3-oxobutanoate, ethyl 2-(2-methylimidazo[2,1-b]thiazol-6-yl)acetate (**4-2**) was obtained via two steps[51] and was directly hydrolyzed in acidic conditions to provide the acid (**4-3**). Introduction of methyl group on **4-2** with CH_3I/NaH followed by ester hydrolysis in basic conditions provided the acid **13-2**. Both acid intermediates were treated with DPPA in toluene followed by reaction with *N*,1-dimethylpiperidin-4-amine to provide the imidothiazole derivatives (**13**, **14**).

Scheme 5. Synthesis of "Imidothiazole" Family Analogues

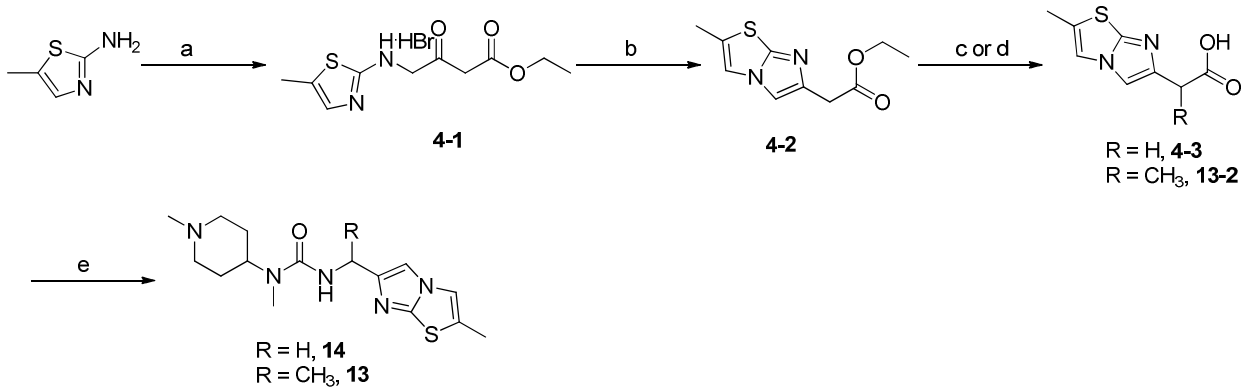

Reagents and conditions: (a) ethyl 4-bromo-3-oxobutanoate, acetone, rt, overnight, 59%; (b) EtOH, reflux, 4h, 97%; (c) conc. HCl, reflux, 10h, 83%; (d) (i) NaH/MeI, DMF, 0°C~rt, 38%; (ii) LiOH aq, MeOH, rt, 3h, quantitatively; (e) *N*,1-dimethylpiperidin-4-amine hydrochloride, DPPA/TEA, toluene, 120°C, overnight, 3% for **13** and 28% for **14**;

The synthesis of piperidine family analogues is outlined in Scheme 6 and Scheme 7. Three approaches were used to make this series of compounds. First, various benzylic amines reacted with triphosgene, then treated with *tert*-butyl 4-(methylamino)piperidine-1-carboxylate followed by deprotection to provide the key urea scaffolds (**11-2**, **12-2**, **19-2**, **22-2** and **37-2**). Reductive amination of these scaffolds with various substituted 2,3-dihydro-1H-inden-1-ones provided the final piperidine derivatives (**11**, **12**, **22**, **37**, and **38**). Starting from the iodide scaffolds, the corresponding ethynyl (**19**, **40**) and ethynylcyclopropane derivatives (**29, 30** and **31**) were obtained by general Sonogashira coupling method and compound **8** was obtained by Stille coupling (Scheme 6).

Scheme 6. Synthesis of "Piperidine" Family Analogues

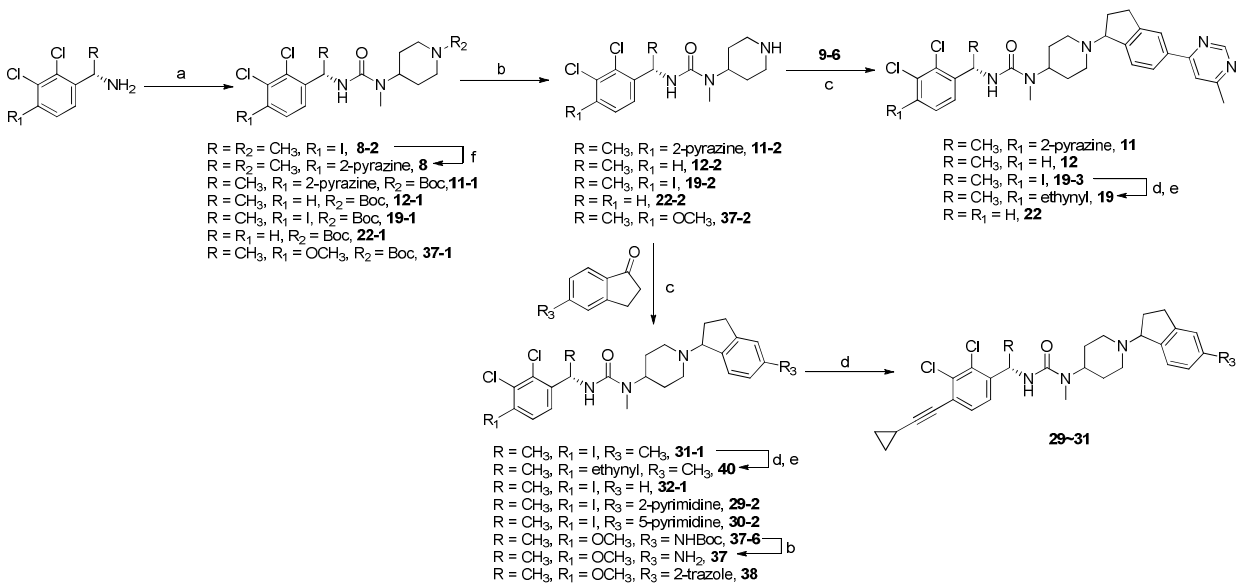

Reagents and conditions: (a) *tert*-butyl 4-(methylamino)piperidine-1-carboxylate, BTC, TEA, DCM, 0ºC~rt, 11~98% yield; (b) TFA/DCM or MeOH/HCl, rt; (c) $Ti(i\text{-}PrO)_4$, THF, reflux, 5h, then $NaBH_3CN$, 50ºC, 2h to overnight, 5~36%; (d) $Pd(PPh_3)_2Cl_2$, ethynyltrimethylsilane or ethynylcyclopropane, CuI, TEA, THF, 80ºC, overnight, 34~81%; (e) K_2CO_3, MeOH, rt, 100%; (f) 2-(tributylstannyl)pyrazine, $Pd(PPh_3)_4$, CuI, DME, 100ºC, overnight, 44%.

Using a similar protocol, compounds **15**, **16**, **17**, **18**, **20**, **21**, **25**, **33**, **34**, **35** **36** and **46**) were obtained by reaction of various benzylic amines with 5-substituted (2,3-dihydro-1H-inden-1-yl)-N-methylpiperidin-4-amines in the presence of triphosgene. Derivatives (**23**, **24**, **26**, **27** and **28**) were prepared by reacting a phenylacetic acid with DPPA followed by treatment with **15-4** according to the alternative approach (Scheme 7).

Scheme 7. Synthesis of "Piperidine" Family Analogues by alternative routes

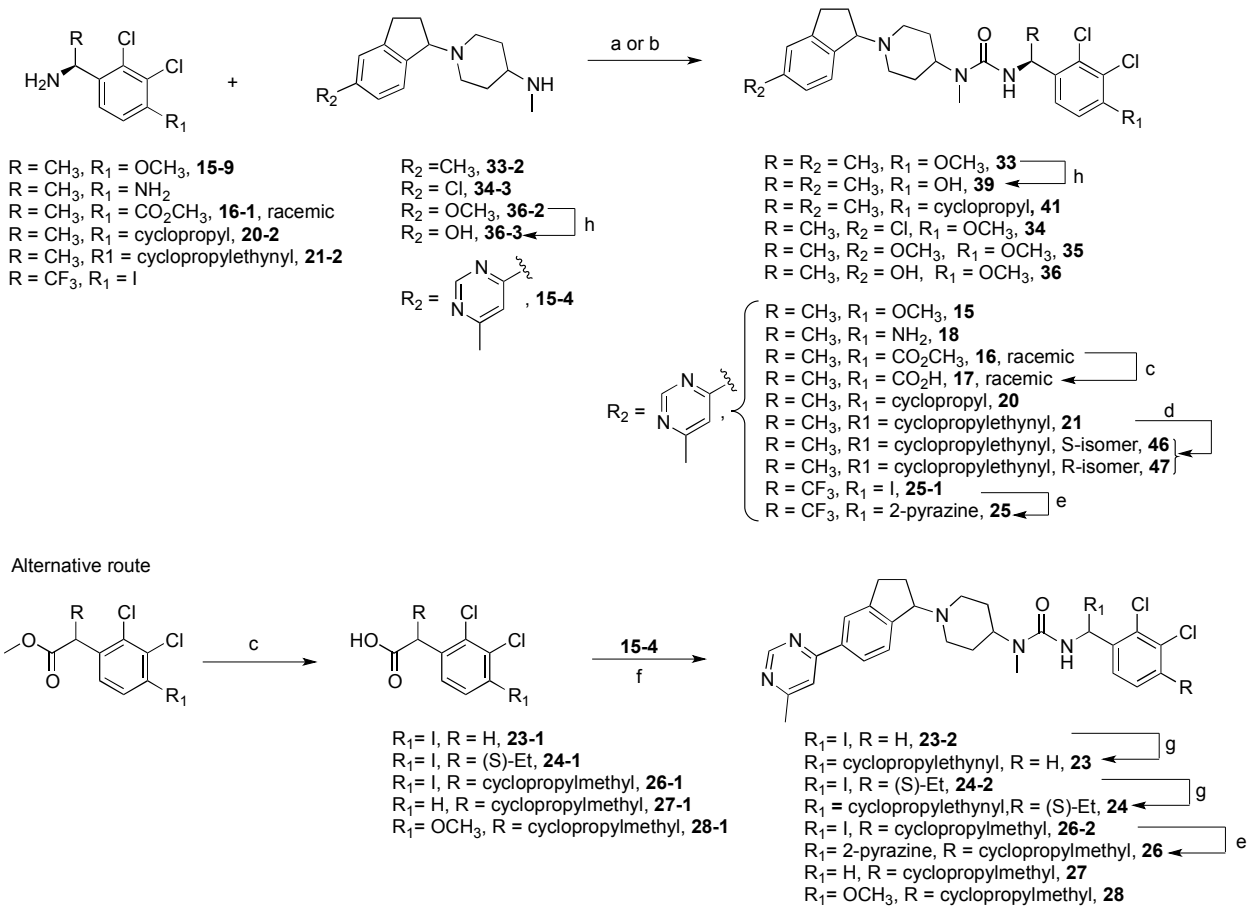

Reagents and conditions: (a) BTC, TEA, DCM, 0 °C~rt, 4~93% yield; (b) CDI, TEA, DCM, 35 °C, overnight, 25% for **18**; (c) LiOH, THF/H_2O or MeOH/H_2O, rt, 3h~overnight, 16-100%; (d) chiral separation by HPLC; (e) 2-(tributylstannyl)pyrazine, $Pd(PPh_3)_4$, CuI, DME, 100°C, overnight, 19~30%; (f) DPPA, TEA, toluene, 120°C, overnight, 49~87%; (g) $Pd(PPh_3)_2Cl_2$, ethynyltrimethylsilane or ethynylcyclopropane, CuI, TEA, THF, 80°C, overnight, 60~89%; (h) BBr_3/DCM, 0°C~rt, 42~54%.

The synthesis of the analogues with other cores is outlined in Scheme 8. Compounds (**43**, **44** and **45**) were prepared from reaction of **8-1** with pyrrolidin- or substituted piperidin-amines via three steps by using similar protocol as synthesis of compound **19**.

Scheme 8. Synthesis of the Analogues with Other Cores

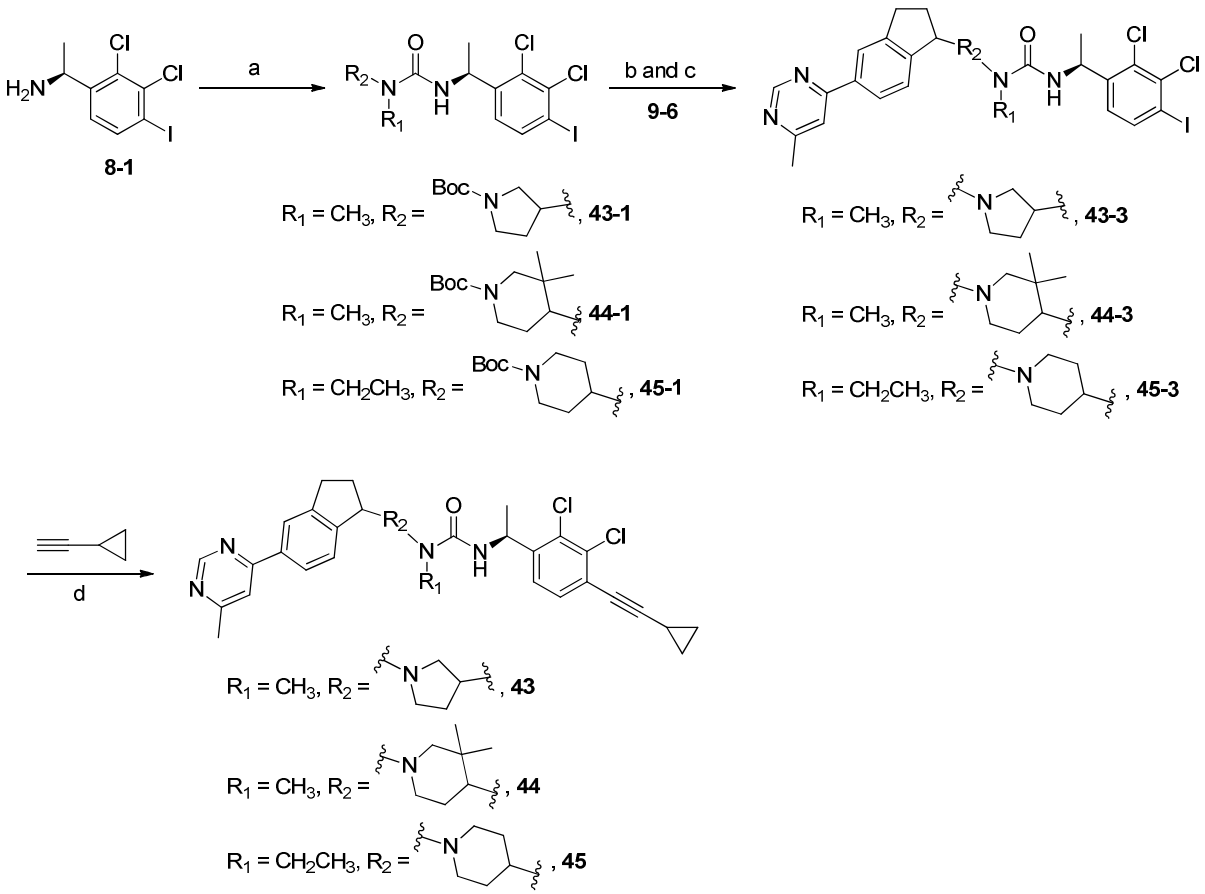

Reagents and conditions: (a) various amines, BTC, TEA, DCM, 0°C~rt, 31~89% yield; (b) TFA/DCM, rt, 87~100%; (c) Ti(*i*-PrO)$_4$, THF, reflux, 5h, then $NaBH_3CN$, 50°C, 2h to overnight, 27~63%; (d) $Pd(PPh_3)_2Cl_2$, CuI, TEA, THF, 80°C, overnight, 13~25%;

CONCLUSION

Starting from a structure-based hypothesis grounded on the superimposition of one inverse agonist and one antagonist computed inside a GHSR model, chimeric design enabled the discovery of a novel chemotype of GHSR-IA. So far, structure-activity and structure-property relationship analyses led to **47** as the best compound with high inverse agonism and antagonism potency in cellular assays. Molecular modeling described a binding mode to ghrelin receptor deeper in the cavity, in agreement with current understanding of GHSR pharmacodynamics. Molecule **47** displays different physicochemical and ADME properties (bigger, more lipophilic, reduced apparent polarity) in comparison with published GHSR-IA. Accordingly, distinct PK

from the state-of-the art is expected. In particular, **47** is anticipated as a moderately orally bioavailable compound in human with high CNS exposure. First *in vivo* studies demonstrated effective reduction of food intake in mouse. Further preclinical studies are on-going to evaluate the most suited mode of administration and to generate final decision-making criteria to nominate what would be, to the best of our knowledge, the first central-acting GHSR-IA in development.

EXPERIMENTAL SECTION

1. Synthesis.

1.1. General Chemistry Procedure. All solvents and chemicals used were reagent grade and supplied by commercial sources unless stated otherwise. Purity and characterization of molecules were established by a combination of liquid chromatography−mass spectroscopy (LCMS), high resolution mass spectroscopy (HRMS) and nuclear magnetic resonance (NMR) analytical techniques. All compounds were measured with at least 95% purity before for testing. ^{1}H NMR and ^{13}C NMR spectra were recorded on Bruker AVANCE300, or AVANCE400 spectrometers (Bruker Company, Germany), using TMS as an internal standard and $CDCl_3$ or DMSO-*d6* as solvents. Chemical shifts are given in ppm(δ). Silica gel thin-layer chromatography was performed on pre-coated plates GF-254 (Qingdao Haiyang Chemical, China), which were visualized by the extinction of UV fluorescence, and/or by staining with KMnO4, followed by heating. Column chromatography was performed using Merck 200-400 mesh silica gel. LCMS was taken on a quadrupole Mass Spectrometer on Agilent LC/MSD 1200 Series (Column: Ultimate XB-C18 (50 × 4.6 mm, 5 μm) operating in ES (+) or (-) ionization mode; T = 30 °C; flow rate = 1.5 mL/min; detected wavelength: 214 or 254 nm). High resolution mass spectra

were recorded by electron spray ionisation at 70 eV on an Agilent G6520 Q-TOF instrument. Prep-HPLC was performed at conditions: (Flash: Welchrom C18, 150 x 20 mm); Wavelength 220 nm; Mobile phase: A MeCN (0.1% TFA); B water (0.1% TFA). Chiral HPLC was performed at conditions: (chiralcel OJ-H, or Chiralpak IA, 250 mm × 4.6 mm, 5 μm; mobile phase: hexane/ethanol/diethylamine = 90:10:0.3; Flow rate: 1.0 mL/min; Wavelength: 230 nm; T = 30 °C).

1.2. Synthesis of representative compounds.

1.2.1. Synthesis of compounds **4**, **9** and **10**

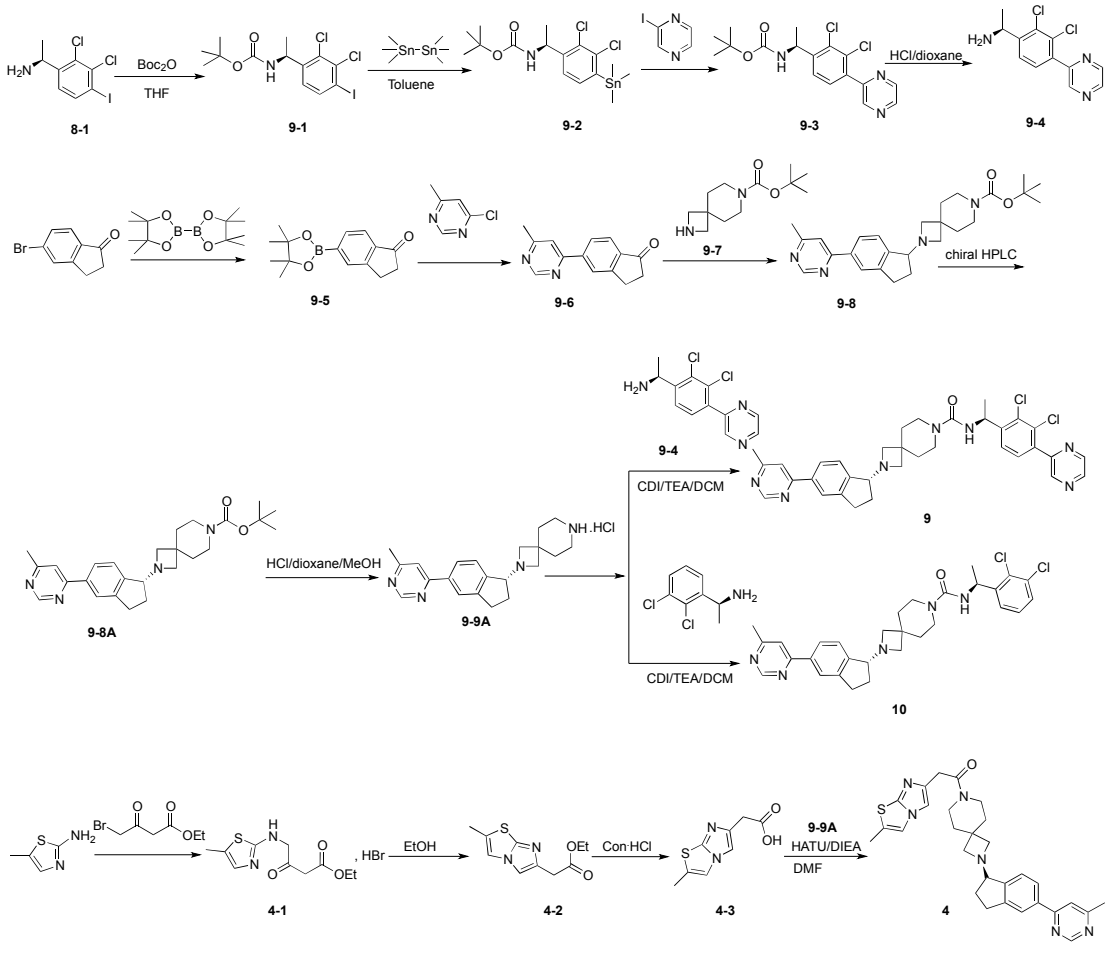

Ethyl 4-((5-methylthiazol-2-yl)amino)-3-oxobutanoate hydrobromide (4-1)

To a solution of 5-methylthiazol-2-amine (3.0 g, 26.4 mmol) in acetone (50 mL) was added a solution of ethyl 4-bromo-3-oxobutanoate (6.9 g, 33.0 mmol) in acetone (40 mL). The mixture was stirred at room temperature overnight. TLC indicated that the reaction was completed. The reaction mixture was filtered. The filter cake was washed with acetone and dried over $MgSO_4$, filtered and concentrated in vacuum to give the title compound **4-1** (5.0 g, 59%) as a white solid.

Ethyl 2-(2-methylimidazo[2,1-b]thiazol-6-yl)acetate (4-2)

A solution of compound **4-1** (5.0 g, 15.5 mmol) in EtOH (125 mL) was stirred at refluxing temperature for 4 h, until the turbid mixture became clear. TLC indicated that the reaction was completed. Then ethanol was removed in vacuum and the residue was dissolved in DCM. The organic layer was washed with solution of sat.$NaHCO_3$, dried over Na_2SO_4 and concentrated in vacuum to afford ethyl 2-(2-methylimidazo[2,1-b]thiazol-6-yl)acetate **4-2** (3.4 g, 97%) as yellow oil.

2-(2-Methylimidazo[2,1-b]thiazol-6-yl)acetic acid hydrochloride (4-3)

A solution of ethyl 2-(2-methylimidazo[2,1-b]thiazol-6-yl)acetate **4-2** (1.5 g, 6.7 mmol) in conc. HCl (15 mL) was stirred at refluxing temperature for 10 h. LCMS indicated that the reaction was completed. Then the solvent of the reaction mixture was removed in vacuum. EtOH (6 mL) was added to dissolve the residue, and a little bit of solid appeared. Then ether (13 mL) was added to the mixture, and it was stirred at room temperature. Ether (13 mL) was decanted out and repeated twice. The solid was dried to afford compound **4-3** (1.3 g, 83%) as a yellow solid.

(R)-2-(2-methylimidazo[2,1-b]thiazol-6-yl)-1-(2-(5-(6-methylpyrimidin-4-yl)-2,3-dihydro-1H-inden-1-yl)-2,7-diazaspiro[3.5]nonan-7-yl)ethanone (4)

The mixture of compound **9-9A** (570 mg, 1.54 mmol), 2-(2-methylimidazo[2,1-b]thiazol-6-yl)acetic acid **4-3** (320 mg, 1.63 mmol), HATU (910 mg, 2.393 mmol) and DIEA (1 mL) in DMF (10 mL) was stirred at room temperature for 2 h. The reaction mixture was concentrated in vacuum. The residue was extracted with EtOAc three times. The combined organic layers were dried over Na_2SO_4, filtered and concentrated in vacuum. The residue was purified by column chromatography on a silica gel column to give the title compound **4** (500 mg, 63%) as a white solid.

^{1}H NMR (400 MHz, $CDCl_3$): δ ppm 9.10 (s, 1H), 7.94 (s, 1H), 7.85 (d, J = 8.0 Hz, 1H), 7.37 (d, J = 8.0 Hz, 1H), 7.27 (d, J = 6.0 Hz, 2H), 7.06 (s, 1H), 3.98-3.96 (m, 1H), 3.77 (s, 2H), 3.55-3.52 (m, 4H), 3.18-3.12 (m, 5H), 2.58 (s, 3H), 2.39 (s, 3H), 2.27-2.24 (m, 1H), 1.96-1.93 (m, 2H), 1.73-1.70 (m, 4H). ^{13}C NMR (100 MHz, CD3OD) δ ppm 170.9, 169.2, 165.6, 159.1, 150, 147.3, 146.9, 141.5, 137.7, 127.6, 126.8, 126.2, 124.9, 118.1, 117.5, 112.3, 72.8, 63.4, 44.7, 40.4, 37.2, 36.5, 35.2, 31.3, 30.4, 23.9, 13.7； HRMS: calc'd for C29H32N6OS $(M+H)^+$, 513.2431; found, 513.2441.

***tert*-Butyl (1-(2,3-dichloro-4-iodophenyl)ethyl)carbamate (9-1)**

A solution of (S)-1-(2,3-dichloro-4-iodophenyl)ethanamine **8-1** (632 mg, 2.0 mmol), $(Boc)_2O$ (872 mg,4 mmol) and Na_2CO_3 solution (3 M, 5 mL) in THF (15 mL) was stirred at room temperature for 2 h. Then the reaction mixture was extracted with EtOAc. The combined organic

layers were washed with brine, dried over Na_2SO_4, filtered and concentrated. The residue was washed with PE to give the title compound **9-1** (375 mg, 45%) as a white solid.

***tert*-Butyl (1-(2,3-dichloro-4-(trimethylstannyl)phenyl)ethyl)carbamate (9-2)**

A mixture of *tert*-Butyl (1-(2,3-dichloro-4-iodophenyl)ethyl)carbamate **9-1** (1.28 g, 3.1 mmol), 1,1,1,2,2,2-hexamethyldistannane (1.5 g, 4.6 mmol), $Pd(PPh_3)_4$ (359 mg, 0.31 mmol) and $(n\text{-}Bu)_4NI$ (1.14 g, 3.1 mmol) in toluene (40 mL) was stirred at refluxing temperature for 4 h. The reaction mixture was concentrated in vacuum. The residue was purified by silica gel column (PE/EtOAc = 30/1, v/v) to afford the title compound **9-2** (602 mg, 43%) as a yellow solid.

(S)-*tert*-butyl (1-(2,3-dichloro-4-(pyrazin-2-yl)phenyl)ethyl)carbamate (9-3)

A mixture of Compound **9-2** (150 mg, 0.33 mmol), 2-iodopyrazine (123 mg, 0.59 mol), $Pd(PPh_3)_4$ (38 mg, 0.033 mmol) and CuI (11 mg, 0.059 mmol) in DME (10 mL) was stirred at 110 °C overnight. The reaction mixture was extracted with EtOAc. The combined organic layers were washed with brine, dried over Na_2SO_4 and concentrated in vacuum. The residue was purified by TLC eluting with PE/ EtOAc (6/1, v/v) to afford compound **9-3** (32 mg, 36%) as a yellow solid.

(S)-1-(2,3-dichloro-4-(pyrazin-2-yl)phenyl)ethanamine (9-4)

The solution of **(**S)-*tert*-butyl (1-(2,3-dichloro-4-(pyrazin-2-yl)phenyl)ethyl)carbamate **9-3** (400 mg, 1.1 mmol) in HCl/dioxane (4 M, 5 mL) was stirred at room temperature for 0.5 h. The reaction mixture was concentrated in vacuum to give the crude compound **9-4** (294 mg, quantitatively) as yellow oil.

5-(4,4,5,5-Tetramethyl-1,3,2-dioxaborolan-2-yl)-2,3-dihydro-1H-inden-1-one (9-5)

To a solution of 5-bromo-2,3-dihydro-1H-inden-1-one (2.0 g, 9.5 mmol) in dioxane (40 mL) was added $Pd(PPh_3)Cl_2$ (199 mg, 0.284 mmol). The mixture was heated to 70 °C. Then to this reaction mixture was added 4,4,4',4',5,5,5',5'-octamethyl-2,2'-bi(1,3,2-dioxaborolane) (4.8 g, 19 mmol) and CH_3COOK (1.85 g, 19 mmol). The reaction mixture was heated to 80 °C overnight. The reaction mixture was extracted with EtOAc. The organic layer was washed with brine, dried over Na_2SO_4 and concentrated in vacuum. Half of the residue was purified by silica gel eluting with DCM/PE (~1/1, v/v) to give the pure product **9-5** (420 mg) as a white solid and the crude product **9-5** (290 mg), yield: 29%.

5-(6-Methylpyrimidin-4-yl)-2,3-dihydro-1H-inden-1-one (9-6)

To a suspension of **9-5** (200 mg, 0.78 mmol), 4-chloro-6-methylpyrimidine (152 mg, 1.17 mmol) and Na_2CO_3 (331 mg, 3.12 mmol) in dioxane/H_2O (10/1, 10 mL) was added $Pd(PPh_3)_4$ (90 mg, 0.078 mmol) under N_2. The reaction mixture was heated to reflux overnight. The mixture was extracted with EtOAc. The organic layer was washed with brine, dried over Na_2SO_4 and concentrated in vacuum. The residue was purified by silica gel eluting with PE/EtOAc (PE to 2/1, v/v) to afford 5-(6-methylpyrimidin-4-yl)-2,3-dihydro-1H-inden-1-one **9-6** (110 mg, 64%) as a white solid.

***tert*-Butyl 2-(5-(6-methylpyrimidin-4-yl)-2,3-dihydro-1H-inden-1-yl)-2,7-diazaspiro[3.5] nonane-7-carboxylate (9-8)**

To a solution of 5-(6-methylpyrimidin-4-yl)-2,3-dihydro-1H-inden-1-one **9-6 (**3.26 g, 14.6 mmol), *tert*-butyl 2,7-diazaspiro[3.5]nonane-7-carboxylate **9-7** (3.29 g, 14.6mmol) and CH_3COONa (4.0 g, 58.8 mmol) in MeOH (100 mL) was added $NaBH_3CN$ (9.2 g, 146 mmol) at 0 ^oC. The reaction mixture was stirred at 0 °C for 2 days and allowed to warm to room temperature. The reaction mixture was adjusted pH = 8 with Na_2CO_3. Then methanol was removed and the residue was extracted with DCM. The organic layer was concentrated in vacuum. The residue was purified by silica gel column to give **9-8** (2.9 g, 46%) as a white solid.

(R)-*tert*-butyl 2-(5-(6-methylpyrimidin-4-yl)-2,3-dihydro-1H-inden-1-yl)-2,7-diazaspiro[3.5] nonane-7-carboxylate (9-8A)

The compound **9-8** (2.9 g) was separated by chiral HPLC to give compound **9-8A** (1.4 g) as a white solid.

(R)-*tert*-butyl 2-(5-(6-methylpyrimidin-4-yl)-2,3-dihydro-1H-inden-1-yl)-2,7-diazaspiro[3.5] nonane-7-carboxylate (9-9A)

The solution of **9-8A** (270 mg, 0.62 mmol) in HCl/dioxane (4 M, 5 mL) and MeOH (5 mL) was stirred at room temperature for 0.5 h. The reaction mixture was concentrated in vacuum to give the crude compound **9-9A** (230 mg, 100%) as yellow oil.

(R)-*tert*-butyl 2-(5-(6-methylpyrimidin-4-yl)-2,3-dihydro-1H-inden-1-yl)-2,7-diazaspiro[3.5] nonane-7-carboxylate (9)

To a solution of (S)-1-(2,3-dichloro-4-(pyrazin-2-yl)phenyl)ethanamine **9-4** (30 mg, 0.11 mmol) in DCM (1.5 mL) was added CDI (22 mg, 0.13 mmol) at 35 °C. The mixture was stirred

at 35 °C for 2.5 h. TEA (0.3 mL) and **9-9A** (55 mg, 0.17 mmol) were added. The resulting solution was stirred for 2 h. The reaction mixture was extracted with EtOAc. The organic layer was washed with Na_2CO_3 solution, dried over Na_2SO_4 and concentrated in vacuum. The residue was purified by silica gel column to afford **9** (51.9 mg, 37%) as a yellow solid.

^{1}H NMR (400 MHz, $CDCl_3$): δ ppm 9.04 (d, *J* = 1.2 Hz, 1H), 8.82 (d, *J* = 1.2 Hz, 1H), 8.60 (t, *J* = 2.4 Hz, 1H), 8.50 (d, *J* = 2.4 Hz, 1H), 7.79 (d, *J* = 8.8 Hz, 1H), 7.61 (s, 1H), 7.48 (s, 1H), 7.38 (d, *J* = 8.0 Hz, 1H), 7.32 (t, *J* = 8.8 Hz, 2H), 5.27(t, *J* = 6.8 Hz, 1H), 4.85 (d, *J* = 5.6 Hz, 1H), 3.93 (t, *J* = 6.8 Hz, 1H), 3.45 (s, 3H), 3.27-3.24 (m, 4H), 3.19-3.10 (m, 4H), 2.52 (s, 3H), 1.54-1.53 (m, 4H), 1.37-1.36 (m, 4H). HRMS: calc'd for C34H35Cl2N7O $(M+H)^+$, 628.2353; found, 628.2353.

N-((S)-1-(2,3-dichlorophenyl)ethyl)-2-((R)-5-(6-methylpyrimidin-4-yl)-2,3-dihydro-1H-inden-1-yl)-2,7-diazaspiro[3.5]nonane-7-carboxamide (10)

To a solution of (S)-1-(2,3-dichlorophenyl)ethanamine (28 mg, 0.15 mmol) in dry DCM (3.0 mL) was added CDI (28 mg, 0.18 mmol) at 0 °C. The mixture was stirred at 35 °C for 2 h. TEA (0.3 mL) and **9-9A** (75 mg, 0.22 mmol) were added. The resulting solution was stirred for 2 h. The reaction mixture was extracted with DCM. The organic layer was washed with Na_2CO_3 solution, dried over Na_2SO_4 and concentrated in vacuum. The residue was purified by prep-TLC to afford **10** (20 mg, 24%) as colorless oil.

^{1}H NMR (400 MHz, CD_3OD): *δ* ppm 9.13 (s, 1H), 8.01 (s, 1H), 7.92 (d, *J* = 7.6 Hz, 1H), 7.61-7.57 (m, 2H), 7.35-7.33 (m, 1H), 7.28-7.24 (m, 1H), 7.17 (t, *J* = 8.0 Hz, 1H), 5.17 (d, *J* = 6.4 Hz,

1H), 4.41 (s, 1H), 3.53 (s, 4H), 3.32-3.26 (m, 5H), 3.02-2.94 (m, 1H), 2.61 (s, 3H), 2.40-2.36 (m, 1H), 2.25-2.21 (m, 1H), 1.84 (s, 4H), 1.44 (d, J = 7.2 Hz, 3H). HRMS: calc'd for C30H33Cl2N5O $(M+H)^+$, 550.2135; found, 550.2141.

1.2.2. Synthesis of compounds **15**, **16**, **17** and **18**

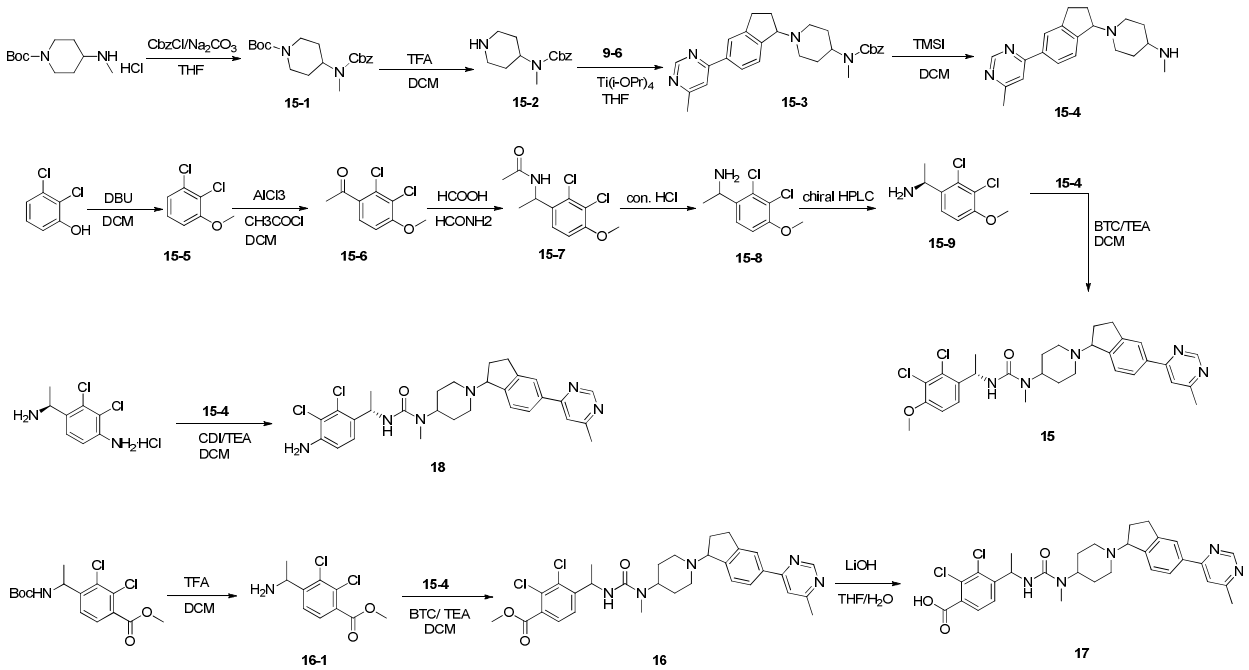

***tert*-Butyl 4-(((benzyloxy)carbonyl)(methyl)amino)piperidine-1-carboxylate (15-1)**

To a solution of *tert*-butyl 4-(methylamino)piperidine-1-carboxylate hydrochloride (1.0 g, 4 mmol) in THF (8 mL) and saturated Na_2CO_3 solution (7 mL) was added a solution of CbzCl (816 mg, 4.8 mmol) in THF (7 mL) drop wise at 0 °C. The reaction mixture was warmed to room temperature for 3 h. The mixture was extracted with EtOAc. The organic layer was washed with brine, dried over Na_2SO_4 and concentrated under vacuum. The residue was purified by

silica gel column (EtOAc/PE = 1/10 to 1/3) to afford compound **15-1** (1.1 mg, 80%) as a white solid.

Benzyl methyl(piperidin-4-yl)carbamate (15-2)

To a solution of **15-1** (1.1 g, 3.16 mmol) in DCM (15 mL) was added TFA (5 mL) slowly at 0 °C. The reaction mixture was stirred at 0 °C for 3 h. The reaction mixture was neutralized with $NaHCO_3$ solution, adjusted to pH = 9 and extracted with DCM. The organic layers were combined, washed with brine, dried over sodium sulfate, filtered and concentrated to afford the crude compound **15-2** (860 mg, 100%) as a white semi-solid.

Benzyl methyl(1-(5-(6-methylpyrimidin-4-yl)-2,3-dihydro-1H-inden-1-yl)piperidin-4-yl) carbamate (15-3)

To a solution of **15-2** (650 mg, 2.6 mmol) and 5-(6-methylpyrimidin-4-yl)-2,3-dihydro-1H-inden-1-one (600 mg, 2.67 mmol) in THF (45 mL) was added Ti(*i*-OPr)$_4$ (4.56 g, 16 mmol) at room temperature under nitrogen atmosphere slowly. The mixture was stirred at refluxing temperature for 5 h. After the reaction mixture was cooled to room temperature, $NaBH_3CN$ (200 mg, 3.17 mmol) was added to the stirring mixture. Then the reaction mixture was stirred at 50 °C overnight. The reaction mixture was neutralized with $NaHCO_3$ solution and extracted with EtOAc. The organic layers were combined, washed with brine, dried over sodium sulfate, filtered and concentrated. The residue was purified by silica column chromatography (DCM/MeOH = 80/1 to 30/1) to afford compound **15-3** (730 mg, 61%) as a yellow solid.

N-methyl-1-(5-(6-methylpyrimidin-4-yl)-2,3-dihydro-1H-inden-1-yl)piperidin-4-amine (15-4)

To a solution of **15-3** (50 mg, 0.11 mmol) in DCM (2 mL) was added TMSI (160 mg, 0.80 mmol) drop wise at 0 °C for 1 h. Two more drops of TMSI were added to the reaction solution. Then the reaction solution was quenched with MeOH (0.3 mL) after another 1 h and concentrated in vacuum. The residue was dissolved in 1N HCl, washed with ether and basified with $NaHCO_3$. The solution was extracted with DCM, washed with brine, dried over Na_2SO_4 and concentrated in vacuum. The residue was purified by silica gel column chromatography (DCM/MeOH·NH_3 = 50/1 to 10/1) to give the compound **15-4** (20 mg, 57%) as colorless oil.

1,2-Dichloro-3-methoxybenzene (15-6)

To a solution of 2,3-dichlorophenol (5.0 g, 30.6 mmol) in DCM (35 mL) was added DBU (4.67 g, 30.6 mmol). The reaction mixture was heated to reflux for 1 h. Then to this reaction mixture was added toluene (20 mL). The reaction mixture was heated to reflux overnight. The reaction mixture was concentrated. MTBE (40 mL) and 1 N HCl aq. solution was added. The MTBE layer was washed with 1 N HCl aq. solution, sat.K_2CO_3 solution and H_2O. The organic layer was concentrated to give **15-6** (5.14 g, 94.7%) as yellow oil.

1-(2,3-Ddichloro-4-methoxyphenyl)ethanone (15-7)

To a solution of $AlCl_3$ (6.01 g, 45 mmol) in DCM (6 mL) was added CH_3COCl (3.32 g, 42 mmol) drop wise at 10~15 °C under N_2. The reaction mixture was stirred at same temperature for 1 h. To this reaction mixture was added a solution of 1,2-dichloro-3-methoxybenzene **15-6** (5.0 g, 28 mmol). The reaction mixture was stirred for 1 h. The mixture was washed with cold 1 N

HCl and extracted with DCM. The organic layer was washed with brine twice and concentrated under reduced pressure. The residue was washed with EtOH to give compound **15-7** (3.7 g, 60%) as a yellow solid.

(S)-1-(2,3-dichloro-4-methoxyphenyl)ethanamine (15-9)

A solution of compound **15-7** (6.7 g, 30.6 mmol) and $HCONH_2$ (7.43 g, 165.2 mmol) in HCOOH (3.87 g, 60.3 mmol) was heated to 160~170 °C for 3 h. The reaction mixture was concentrated and cooled to 70 °C. To the reaction mixture was added conc. HCl (15 mL) and water (14 mL). The mixture was heated 100 °C overnight. The reaction mixture was cooled and added 50% aq. NaOH solution to adjust pH = 13. The mixture was extracted with DCM. The organic layer was washed with brine and concentrated to give the crude compound, which was purified by HPLC to give pure compound 1-(2,3-dichloro-4-methoxyphenyl)ethanamine (6.0 g, 90%) as yellow oil. It was separated by chiral HPLC to give *S*-enantiomer **15-9** (3.2 g) as a yellow solid.

3-((S)-1-(2,3-dichloro-4-methoxyphenyl)ethyl)-1-methyl-1-(1-(5-(6-methylpyrimidin-4-yl)-2,3-dihydro-1H-inden-1-yl)piperidin-4-yl)urea (15)

To a mixture of (S)-1-(2,3-dichloro-4-methoxyphenyl)ethanamine **15-9** (50 mg, 0.23 mmol) and TEA (0.5 mL) in dry DCM (5.0 mL) was added BTC (61 mg, 0.21 mmol) at 0 °C. Then the reaction was stirred at 0 °C for 20 min. Then a solution of compound **15-4** (80 mg, 0.25 mmol) in dry DCM (1.0 mL) was added. The resulting mixture was stirred at 0 °C for 30 min. LC-MS indicated that the reaction was completed. The reaction mixture was extracted with DCM. The combined organic layer was dried over Na_2SO_4 and concentrated in vacuum. The residue was

purified by silica gel chromatography (5% methanol in dichloromethane) to afford **15** (120 mg, 93%) as a yellow solid.

^{1}H NMR (400 MHz, $CDCl_3$): δ 9.05 (s, 1H), 7.85-7.80 (m, 2H), 7.50 (s, 1H), 7.38 (d, J = 8.1 Hz, 1H), 7.14-7.11 (m, 1H), 6.77-6.74 (m, 1H), 5.19-5.13 (m, 1H), 4.75 (d, J = 6.8 Hz, 1H), 4.36-4.30 (m, 1H), 4.06-3.96 (m, 1H), 3.81 (d, J = 2.8 Hz, 3H), 2.89-2.82 (m, 3H), 2.73 (s, 3H), 2.60-2.52 (m, 4H), 2.39-2.32 (m, 1H), 2.21-2.14 (m, 1H), 2.05-2.02 (m, 2H), 1.70-1.56 (m, 3H), 1.41 (d, J = 6.8 Hz, 3H). HRMS: calc'd for C30H35Cl2N5O2 $(M+H)^+$, 568.2241; found, 568.2253.

Methyl 4-(1-aminoethyl)-2,3-dichlorobenzoate (16-1)

To a stirred solution of methyl 4-(1-((*tert*-butoxycarbonyl)amino)ethyl)-2,3-dichlorobenzoate (160 mg, 0.46 mmol) in DCM (3.0 mL) was added TFA (1.0 mL) at 0 °C. Then the reaction mixture was stirred at 0 °C for 3 h. Upon completion, the reaction mixture was neutralized with Na_2CO_3 solution to pH = 7 at 0 °C. The resulting mixture was extracted with DCM (20 mL x 3). The combined organic layers were washed with brine (20 mL), dried over sodium sulfate, filtered and concentrated to give the title compound **16-1** (112 mg, 99%) as a beige oil.

Methyl 2,3-dichloro-4-(1-(3-methyl-3-(1-(5-(6-methylpyrimidin-4-yl)-2,3-dihydro-1H-inden -1-yl)piperidin-4-yl)ureido)ethyl)benzoate (16)

To a mixture of methyl 4-(1-aminoethyl)-2,3-dichlorobenzoate **16-1** (60 mg, 0.25 mmol) and TEA (1.0 mL) in dry DCM (10.0 mL) was added compound **15-4** (100 mg, 0.31 mmol) at 0 °C, then a solution of BTC (60 mg, 0.20 mmol) in dry DCM (1.0 mL) was slowly added. The resulting mixture was stirred at room temperature overnight. Upon completion, the reaction

mixture was diluted with DCM. The combined organic layer was washed with brine, dried over Na_2SO_4 and concentrated in vacuum. The residue was purified by silica gel chromatography (2-10% methanol in dichloromethane) to afford **16** (50 mg, 35%) as white solid.

^{1}H NMR (400 MHz, $CDCl_3$): δ ppm 9.12 (s, 1H), 7.96 (s, 1H), 7.89 (d, J = 7.6 Hz, 1H), 7.63-7.60 (m, 1H), 7.56 (s, 1H), 7.29-7.26 (m, 2H), 5.34-5.26 (m, 1H), 4.86 (s, 1H), 4.57-4.50 (m, 1H), 4.24-4.17 (m, 1H), 3.91 (d, J = 2.8 Hz, 3H), 3.08-2.85 (m, 7H), 2.59-2.49 (m, 5H), 2.27-2.18 (m, 2H), 1.70-1.59 (m, 4H), 1.46 (d, J = 7.2 Hz, 3H). HRMS: calc'd for C31H35Cl2N5O3 $(M+H)^+$, 596.219; found, 596.2195.

2,3-dichloro-4-(1-(3-methyl-3-(1-(5-(6-methylpyrimidin-4-yl)-2,3-dihydro-1H-inden-1-yl)piperidin-4-yl)ureido)ethyl)benzoic acid (17)

To a stirred solution of **16** (23 mg, 0.04 mmol) in THF/H_2O (3 mL/0.3 mL) was added LiOH (30 mg, 0.73 mmol) at room temperature. The reaction was stirred at room temperature overnight. The reaction mixture was filtered through syringe filter. The filtrate was acidified with 2 drops of conc. HCl and filtered. The organic layer was concentrated, washed with DCM/PE to give compound **17** (3.4 mg, 16%) as a white solid.

^{1}H NMR (400 MHz, CD_3OD): δ 9.15 (s, 1H), 8.24-8.20 (m, 2H), 8.10 (s, 1H), 7.87 (d, J = 8.4 Hz, 1H), 7.68-7.66 (m, 1H), 7.43-7.41 (m, 1H), 5.34-5.27 (m, 2H), 5.07-5.05 (m, 1H), 4.25 (br s, 1H), 3.52-3.51 (m, 1H), 3.13-3.12 (m, 2H), 2.89 (s, 3H), 2.66 (s, 3H), 2.61-2.58 (m, 2H), 2.21-2.17 (m, 2H), 2.03-2.02 (m, 2H), 1.85-1.67 (m, 2H), 1.60-1.59 (m, 1H), 1.45-1.44 (m, 3H). LC-MS: Rt = 2.428 min, $[M+H]^+$: 582.3.

3-((S)-1-(4-amino-2,3-dichlorophenyl)ethyl)-1-methyl-1-(1-(5-(6-methylpyrimidin-4-yl)-2,3-dihydro-1H-inden-1-yl)piperidin-4-yl)urea (18)

To a stirred mixture of (S)-4-(1-aminoethyl)-2,3-dichloroaniline hydrochloride (50 mg, 0.18 mmol) and TEA (0.2 mL) in dry DCM (5 mL) was added CDI (44 mg, 0.27 mmol) at room temperature. The mixture was stirred at 35 °C for 3 h. Then compound **15-4** (116 mg, 0.36 mmol) in dry DCM (1 mL) was added. The resulting mixture was stirred at 35 °C overnight. LC-MS indicated that the reaction was completed. The reaction mixture was extracted with DCM. The organic layer was dried over Na_2SO_4 and concentrated in vacuum. The residue was purified by prep-TLC to afford compound **18** (24.5 mg, 25%) as yellow solid.

^{1}H NMR (400 MHz, $CDCl_3$): δ 9.14 (s, 1H), 8.03 (s, 1H), 7.91 (d, J = 7.6 Hz, 1H), 7.57 (s, 1H), 7.26 (s, 1H), 7.01 (d, J = 8.8 Hz, 1H), 6.67-6.64 (m, 1H), 5.20-5.15 (m, 1H), 4.81 (d, J = 4.4 Hz, 1H), 4.51-4.43 (m, 1H), 4.13-4.10 (m, 2H), 3.49 (s, 1H), 3.14-3.02 (m, 3H), 2.82-2.40 (m, 12H), 1.78-1.70 (m, 2H), 1.45 (d, J = 6.8 Hz, 3H). HRMS: calc'd for C29H34Cl2N6O $(M+H)^+$, 553.2244; found, 553.2245.

1.2.3. Synthesis of compounds **21**, **46** and **47**

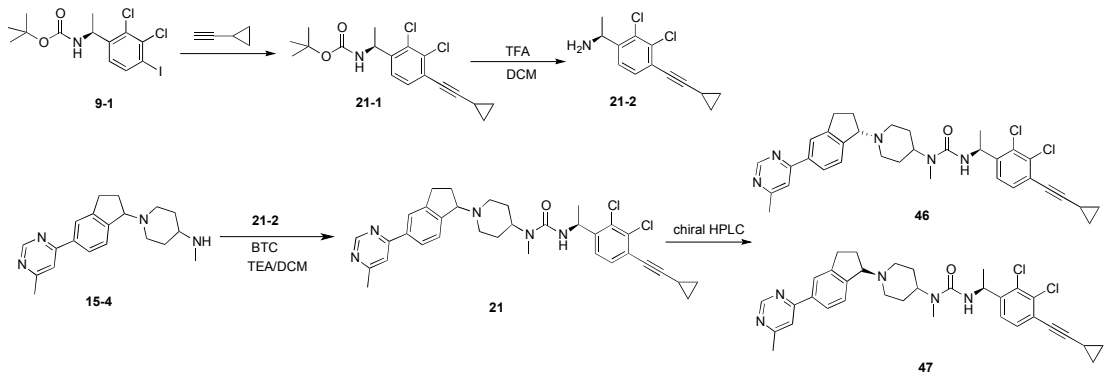

(S)-*tert*-butyl (1-(2,3-dichloro-4-(cyclopropylethynyl)phenyl)ethyl)carbamate (21-1)

To a solution of **9-1** (164 mg, 0.52 mmol), ethynylcyclopropane (171 mg, 2.60 mmol), CuI (32 mg, 0.17 mmol) and TEA (210 mg, 2.08 mmol) in dry THF (10 mL) was added $Pd(PPh_3)_2Cl_2$ (73

mg, 0.10 mmol) at room temperature under N_2 atmosphere. The resulting mixture was heated to 80 °C in a sealed-tube overnight. Then the reaction solution was concentrated in vacuum. To the residue was added water and extracted with EtOAc. The organic layer was washed with brine, dried over Na_2SO_4, filtered and concentrated. The residue was purified by silica column chromatography (DCM/MeOH = 100/1 to 40/1) to afford **21-1** (120 mg, 65%) as a white solid.

(S)-1-(2,3-dichloro-4-(cyclopropylethynyl)phenyl)ethanamine (21-2)

To a solution of **21-1** (130 mg, 0.34 mmol) in DCM (10 mL) was added TFA (3 mL) drop wise at 0 °C. The reaction mixture was stirred at 0 °C until the reaction was completed. The reaction mixture was neutralized with $NaHCO_3$ solution at 0 °C, and extracted with DCM. The organic layers were combined, washed with brine, dried over sodium sulfate, filtered and concentrated. The residue was purified by silica gel column (DCM to DCM/MeOH = 15/1) to afford the compound **21-2** (81 mg, 95%) as a white solid.

3-((S)-1-(2,3-dichloro-4-(cyclopropylethynyl)phenyl)ethyl)-1-methyl-1-(1-(5-(6-methylpyrimidin-4-yl)-2,3-dihydro-1H-inden-1-yl)piperidin-4-yl)urea (21)

To a solution of **21-2** (65 mg, 0.26 mmol) and TEA (1 mL) in DCM (6 mL) was added BTC (89 mg, 0.29 mmol) in portions at 0 °C. The solution was stirred at 0 °C for 15 min. **15-4** (188 mg, 0.29 mmol) was added. The resulting solution was stirred for another 30 min at 0 °C. The reaction mixture was diluted with DCM, washed with Na_2CO_3 solution and brine, dried over Na_2SO_4 and concentrated in vacuum. The residue was purified by silica gel column chromatography, followed by Prep-HPLC to afford **21** (64 mg, 40%) as a white solid.

3-((S)-1-(2,3-dichloro-4-(cyclopropylethynyl)phenyl)ethyl)-1-methyl-1-(1-((S)-5-(6-methylpyrimidin-4-yl)-2,3-dihydro-1H-inden-1-yl)piperidin-4-yl)urea (46) and 3-((S)-1-(2,3-dichloro-4-(cyclopropylethynyl)phenyl)ethyl)-1-methyl-1-(1-((R)-5-(6-methylpyrimidin-4-yl)-2,3-dihydro-1H-inden-1-yl)piperidin-4-yl)urea (47)

The compound **21** (125 mg) was separated by chiral HPLC to give compound **46** (35 mg) as a white solid and compound **47** (20 mg) as a white solid, respectively.

^{1}H NMR of **46** (400 MHz, $CDCl_3$): δ ppm 9.04 (s, 1H), 7.85-7.80 (m, 2H), 7.56 (s, 1H), 7.37 (d, J = 7.6 Hz, 1H), 7.21-7.19 (m, 1H), 7.09-7.04 (m, 1H), 5.21-5.17 (m, 1H), 4.73 (d, J = 6.4 Hz, 1H), 4.32 (t, J = 7.2 Hz, 1H), 4.03-3.97 (m, 1H), 2.93-2.76 (m, 3H), 2.73 (s, 3H), 2.57-2.52 (m, 4H), 2.36 (t, J = 10.4 Hz, 1H), 2.17 (t, J = 10.4 Hz, 1H), 2.07-2.00 (m, 2H), 1.70-1.65 (m, 1H), 1.60-1.36 (m, 7H), 0.93-0.87 (m, 4H). ^{13}C NMR (100 MHz, CD3OD) δ ppm 168.3, 164.9, 158.6, 158.2, 145.9, 145.8, 145.3, 136.7, 134.5, 131.3, 131.1, 126.1, 125.9, 124.4, 123.9, 117.3, 99.9, 72.4, 70.1, 52.8, 50.6, 49.2, 46.7, 42.7, 30.9, 29.4, 28, 25.3, 23, 20.2, 10.7, 8.4. HRMS: calc'd for C34H37Cl2N5O $(M+H)^+$, 602.2448; found, 602.2455.

^{1}H NMR of **47** (400 MHz, CD_3OD): δ ppm 9.00 (s, 1H), 8.01-7.98 (m, 2H), 7.87 (s, 1H), 7.54 (d, J = 7.6 Hz, 1H), 7.33-7.24 (m, 2H), 5.24-5.23 (m, 1H), 4.45-4.42 (m, 1H), 3.98 (br s, 1H), 3.06-3.00 (m, 2H), 2.93-2.91 (m, 1H), 2.84 (s, 3H), 2.74-2.71 (m, 1H), 2.56 (s, 3H), 2.44-2.37 (m, 2H), 2.22-2.17 (m, 2H), 1.57-1.50 (m, 3H), 1.43-1.39 (m, 3H), 1.31-1.27 (m, 2H), 0.95-0.90 (m, 2H), 0.79-0.76 (m, 2H).

2. Molecular Modeling.

Molecular docking was performed for generating structural hypotheses to design chimeric new molecules relying on the superimposition of inverse agonist and antagonist structures inside the

ghrelin receptor (GHSR). Because no experimental structure of GHSR has been made available at the time of writing this manuscript, a theoretical tridimensional model was selected and retrieved from ModBase (https://modbase.compbio.ucsf.edu/ accessed August 2017), a database of comparative protein structure models.[52] The structure was built by homology modeling, based on alignment of protein sequence of gorilla GHSR (366 amino acids, Uniprot ID G3SFQ1 showing 100% identity with human sequence Q92847) and of the rat neurotensine receptor as GPCR crystallographic template (PDB ID 4BUO). The sequence identity was 39.36 % and the final model covers position 46-311. Visual inspection and structural assessment scores allowed us to consider the GHSR model suitable to be employed 'as is' as input of our docking protocol.

Molecular docking of Pfizer GHSR-IA PF-05190457, Helsinn GHSR antagonist H0700 and the designed central-acting GHSR (compounds **4**, **8** and **47** in Figures 1, 2 and 4A respectively) was performed with Attracting Cavities (AC).[35] Briefly, AC principle consists in sampling the ligand posing space by energy minimization only. This is achieved by setting a smooth attracting potential steering the ligands into protein cavities instead of the actual repulsive potential on the surface of the protein. The attractive potential is obtained by placing points in concave region of the protein, which fit the attractive part of Lennard-Jones potential. Other points are necessary to take charges into account inside protein cavities. A first round of minimizations is done on this attracting/electrostatic cloud, and then a final refinement producing the poses takes place after reintroduction of the actual protein potential. AC scores binding modes with a full force-field evaluation of the reformed complexes relying on CHARMM.[53,54] Here, AC was employed following the protocol as detailed in the methodology article.[35] A search space was defined as a rectangular parallelepiped of 24 x 20 x 33 Å, centered on Phe309 side chain with the longer side of the box in the main orientation of the receptor. We set a rotation step of 45° along each axis

after the ligand being centered on every point of the cloud. This way the sampling was expected to be both focused and enhanced. Moreover, flexibility of binding side residues was allowed during AC docking. This was effective for all side chains within 8Å from the initial position on cloud point, during sampling by exploring alternate rotameric positions according to the EBL librairy[55] and minimization. The main aim was to fix some structural uncertainties inherent to any homology model but the protein flexibility revealed a crucial methodological step that enabled the access to the deeper cavity postulated as a determinant for inverse agonism activity and thus to generate the structural hypothesis yielding the novel chimeric GHSR-IA chemotype.

3. Cheminformatics.

All cheminformatic calculations were performed by SwissADME (http://www.swissadme.ch), a web-based tool that gives access to a pool of fast yet robust models for physicochemical properties, pharmacokinetic behaviors, drug-likeness and medicinal chemistry friendliness.[24] Here, molecular, physicochemical, ADME and druglikeness properties were estimated. For lipophilicity, WLOGP is a log *P* predictor based on our own implementation of the fragmental system of Wildman and Crippen.[33] For apparent polarity, the topological polar surface area (TPSA) was obtained following strictly the fragmental method developed by Ertl *et al*.[23]

SwissADME includes a support vector machine (SVM)[56] classification model for predicting the propensity of a compound to be substrate of P-glycoprotein1 (P-gp), an important efflux protein, which pumps out xenobiotics from the CNS. The prediction is based on 16 molecular and physicochemical descriptors from SwissADME. It was built on a curated training set of 1033 molecules. The predictive capability was tested on a set of 215 substrates and 200 non-substrates. The external accuracy, specificity and sensitivity are 89%.

The Bioavailability Radar[24] was produced through SwissADME and enables a rapid appraisal of druglikeness of compounds under study. Six molecular and physicochemical properties are considered and expressed by six descriptors of SwissADME. Ranges of optimal values are depicted as a pink area. For saturation, the ratio of sp^3 hybridized carbons over the total carbon count of the molecule should be at least 0.25. For size, MW should be between 150 and 500 g/mol. For polarity, TPSA should be between 20 and 130Å^2. For solubility, log *S* (calculated with ESOL[46]) should be less than -6. For lipophilicity, XLOGP3[57] should be between -0.7 to +6.0. For flexibility, the molecule should bear less than 10 rotatable bonds. The red radar of the compound must be fully encompassed by the pink area to be considered as druglike and orally bioavailable. Any deviation signifies a suboptimal property for oral bioavailability.

All novel compounds were evaluated for pan assay interference (PAINS) to point out potential frequent hitters or promiscuous compounds, which are molecules containing substructures showing potent response in assays irrespective of the protein target. The 481 recurrent fragments, considered as potentially leading to PAINS compounds[58] are implemented in a pattern recognition algorithm of SwissADME allowing for rapid screening[24]. No warning were returned.

4. Biological protocols.

4.1. Evaluation of inverse agonist potency (EC_{50}) on ghrelin receptor (GHSR) by inositol phosphate accumulation assay (IP-1)

HEK293 cells stably expressing recombinant human GHSR (HEK293/GHSR1a) were used in the *inositol phosphate* (IP-1) HTRF assay. One day before the test, cells were seeded at a density of 1.5×10^4/well in a Matrigel® coated 384-well plate with 30 µL of complete Dulbecco's

Modified Eagle's Medium and incubated at 37 °C in 5 % CO_2 for 18–22 h. On test day, the medium was removed by centrifugation at 600 rpm for 30 s, and 20 µL of stimulation buffer containing 1x tested compound was added with Bravo (Automate liquid handling platform, Agilent Technologies). The plate was then incubated at 37 °C and 5% CO_2 for 1 hour. After the incubation, 5 µL of IP-1 analog coupled to a deuterium fluorophore (IP1-d2 and) 5 µL of Tb-Cryp were added to all wells using Multidrop™ Combi (Thermo Fischer Scientific Inc., United States). After additional incubation at room temperature for 1 h, the plates were read on Envision™ with 620nm and 665nm optical filters (Perkin Elmer Inc., United States).

4.2. Evaluation of antagonist potency (IC_{50}) on ghrelin receptor (GHSR) by intracellular calcium release assay (FLIPR)

The intracellular calcium release assay was carried out in a 384-well fluorescence imaging plate reader (FLIPR™, Molecular Devices LLC, United States) HEK293/GHSR1a cell line. Cells were seeded 24 h prior to the experiments. Pre-incubation with calcium dye lasted for 30-60 min at room temperature or 37 ºC. Test compounds, dissolved in DMSO, were added and incubated for 15 min followed by the addition of ghrelin with FlexStation or FLIPR. Relative fluorescence was monitored by the FLIPR™. IC_{50} values were calculated from dose-response data using Prism software (version 6.07, GraphPad Software, United States). To check for GHSR antagonism, the test compounds and ghrelin (10 nM) were added to the cells at t = 20 s and the calcium response were measured for 2 min. The potency of the antagonist was calculated by its ability to reduce the ghrelin response.

4.3. Inhibition of anamorelin-induced increase of food intake (FI)

This study was performed in accordance with the *Guide for the Care and Use of Laboratory Animals*.[59] Male C57BL/6J mice, with body weight from 18 to 22 g at arrival, were obtained from HDB Shanghai Laboratory. Animals were selected for inclusion in the study based upon acceptable clinical condition and body weight. Animals were housed in pairs in standard propylene cages, lined with wood chip bedding, and were provided with *ad libitum* access to food pellets and tap water. Animals were acclimatized for at least one week in a room controlled for temperature (22 to 26 °C), humidity (30-70%), and lighting (12 h light–dark cycle). At time t = 0, animals were given **47** either 10 mg/kg i.p. (n=6) or 30 mg/kg p.o. (n=6), and t = 10 min, anamorelin 30 mg/kg p.o. The cumulative food intake was measured at time points t = 1, 2, 4, 8 and 24 h, and 0-24 h AUC of FI were calculated for both treatments, for vehicle alone (n=6) and for vehicle plus anamorelin 30 mg/kg (n=6). Vehicle for oral formulation was carboxyl methyl cellulose (CMC 0.5%). Vehicle for parenteral formulation was a mixture of dimethylacetamide (DMAC 10%), Solutol HS 15 (6%) and phosphate buffered saline (PBS 84%). Body weight was measured daily.

4.4. Evaluation of hERG inhibition

In-house generated hERG/HEK293 cells stably expressing human Ether-à-go-go-Related Gene (hERG) channel were cultured at 37 °C, 5% CO2 in Dulbecco's Modified Eagle Media supplemented with 10% fetal bovine serum, 1% penicillin/streptomycin, and 500 μg/mL Geneticin (Invitrogen™, Thermo Fischer Scientific Inc., United States). The hERG inhibition assay was performed by manual patch clamp system using standard whole-cell configuration. The intracellular solution is composed of 130mM KCl, 1.0mM $MgCl_2$, 5.0mM EGTA, 10mM HEPES, 5.0mM Mg-ATP; adjust pH to 7.25 with 1M KOH; osmolarity approximately at 280 mOsm. The extracellular solution contained 137mM NaCl, 1.8mM CaCl2, 1.0mM MgCl2,

4.0mM KCl, 10mM Glucose, 10 mM HEPES; adjust pH to 7.4 with 1M NaOH; osmolarity approximately at 295 mOsm. To elicit hERG current, the cells were depolarized to +40mV for 2 s to activate hERG current, and then clamped to -40mV for 3 s to record a tail current by an amplifier (EPC 10^{TM}, HEKA, Harvard Bioscience Inc., United States). The peak tail current before addition of the compounds were measured as the control hERG current amplitude. Test compound was added and incubated on the cells for a period of 5 min, and then peak tail current was measured as test compound hERG current amplitude. %hERG inhibition was calculated (n=3 or 4) accordingly. All experiments were conducted at room temperature.

4.5. Evaluation of microsomal stability

Incubation mixtures were prepared by mixing liver microsomes (Gentest^{TM}, BD Biosciences, Unites States) of human, rat, mouse and dog, 20 mg/mL of microsomes protein, buffer (50 mM potassium phosphate buffer at pH 7.4) and test item in 4 mL glass tube. Final concentration of incubation mixtures were 0.625 mg/mL liver microsomal protein and 0.625 μM test item. For the 0 min time point sample, 160 μL of the above mixture were added to 40 μL of buffer. Reaction mixtures were pre-incubated at 37 ^{o}C in a water bath for 5 min and then reactions were started by addition of 400 μL NADPH solution (5 mM in 50 mM potassium phosphate buffer). Incubation mixtures were constantly shaken at 37 ^{o}C in water. After 5, 15, 30 and 60 min, 200 μL of the incubation mixtures were added to 400 μL stop reaction mixture (cold MeCN containing 20 ng/mL internal standard). Samples were shaken with a Vortex, centrifuged at 13000 rpm for 10 min and transferred (100 μL of supernatant) to injection plate for LC-MS/MS analysis (API 4000, Analyst 1.5, Applied Biosystems, AB SCIEX, United States). Positive control incubation

mixtures were prepared and treated with the same procedure described above; 0.312 mg/mL liver microsomes and 1.25 μM midazolam final concentrations.

Negative control samples were prepared and treated with same procedure described above; 0.625 mg/mL liver microsomes and 0.625 μM test item final concentrations. Reactions were started by the addition of 400 μL buffer. Standard curves were prepared by using boiled inactivated liver microsomes. The $T_{1/2}$ approach was used for calculation of *in vitro* intrinsic clearance.[60]

*4.6. Pharmacokinetics of compound **47***

This study was performed in accordance with the *Guide for the Care and Use of Laboratory Animals*.[59] For orogastric gavage (o.g.), compound **47** was suspended in vehicle (2% DMSO and 98% of 0.5% carboxymethylcellulose). For intravenous (i.v.) injection, **47** was dissolved in 2% DMSO, 50% of 40% 2-hydroxypropyl-β-cyclodextrin (HP-β-CD) in distilled water. For i.v. and o.g. administration each rat received 3 mg/kg of compound **47** in 3 mL kg^{-1} via tail vein and oral gavage tube, respectively. Repeated blood samples (0.2–0.3 mL) were collected into polypropylene tubes containing EDTA-K_2 at 0.08, 0.25, 0.5, 1, 2, 4, 8, and 24 h after i.v. injection and at 0.25, 0.5, 1, 2, 4, 8, 24 h after o.g. Plasma samples separated by centrifugation were stored at −20°C until analysis. Brain samples were collected after euthanasia by CO_2 inhalation at 2 h following i.v. administration and were homogenized with five-fold volume of phosphate buffer saline (PBS, pH 7.4) and stored at −20°C until analysis. Plasma and brain concentrations of **47** were determined by liquid chromatography tandem mass spectrometry (LC-MS/MS). Brain to plasma (B/P) ratio was calculated by the ratio of brain and plasma concentration at 2 h after i.v. administration. The sample of standard curves and quality controls (QCs) for compound **47** in plasma and homogenized brain are prepared in duplicate. Samples

were mixed with 100% acetonitrile containing 50 ng mL^{-1} internal standard (IS, propranolol), vortexed about 1 min, centrifuged at 4 ^{o}C for 10 min at 13,000 rpm and supernatant was transferred to a 96-well injection plate. Finally, 10 μL samples were injected into LC-MS/MS. The preparation of dose solution and experiment samples wasthe same as standard curve. All samples were analyzed by using LC-MS/MS (mass spectrometer API 4000, AB SCIEX and HPLC Agilant 1200) in multiple reaction monitor (MRM) transition mode equipped with a turbo ion electrospray source working in positive ionization mode. The MRM transitions were: 602.4→157.4 m/z (compound **47**), and 260.3→116.3 m/z (propanolol, IS). Chromatography column was a Sepax GP-C4, (5μm, 2.1×50mm). Mobile phase was 0.1% formic acid in water (Phase A) and 0.1% formic acid in acetonitrile (Phase B) at a flow rate of 0.4 mL/min. The gradient chromatography run started with 10% Phase B that was increased until 90% in 1.5 min with a total time chromatography of 3 min. A weighed quadratic regression function ($1/x^2$) was used to fit calibration lines and to calculate compound **47** concentrations in the calibration range of 5-5000 ng/mL

*4.7. Evaluation of plasma protein binding of compound **47***

Plasma protein binding (PPB) evaluation was performed adding appropriate amounts of the working solutions of compound **47** in DMSO previously prepared to aliquots of plasma samples of human, dog, mouse or rat, in order to obtain the final concentrations of 1.0 μM. The amount of solution added to each sample was 0.5% of the final volume. The concentration in samples before dialysis (T0) was measured by LC-MS/MS. Equilibrium dialysis was performed in a 96-well plate device with 12-14 kD membranes cut-off (HTDialysis LLC, United States); after vortex-mixing, aliquots (150 μL, in triplicate) of fortified plasma samples were loaded into the

equilibrium dialysis donor side. An equivalent volume of DPBS (Dulbecco's Phosphate Buffered Saline, pH 7.4, by Sigma) buffer was loaded into the corresponding half-cell (acceptor side). The plate was sealed and incubated for 6 h at 37 °C in incubator with 5 % CO_2 atmosphere. To evaluate the nonspecific binding, additional control samples were prepared in DPBS buffer at final concentration 1.0 μM and spiked samples were loaded into the equilibrium dialysis device and processed as described above. After incubation, the samples collected from the donor side (used for total drug concentration) and from the acceptor side (containing the unbound drug) were removed from the plate and stored at – 80 °C until LC-MS/MS analysis. The free fraction f_u of the drug in plasma was calculated as follows:

$$f_u = \frac{C_A}{C_D}$$

where C_A and C_D are the concentrations in the acceptor chamber (buffer) and in the donor chamber (plasma) at the end of the dialysis, respectively. Percentages of free fraction (% f_u) and of bound fraction (% f_b) were calculated and PPB is expressed as percentage of binding.

*4.8. Evaluation of apparent permeability (P_{app}) of compound **47** (Transwell Assay).*

hMDRI-MDCK Ⅱ (human Multidrug Resistance Protein - Madin-Darby Canine Kidney transfected) cells were seeded into 24-multiwell Insert Systems with PET (polyethylene terephthalate) membranes (1 μm pore size and 0.3 cm^2 surface area) at an optimized density of 2×105 cells/ml in cell culture medium for four days. Monolayer integrity is checked with TEER (Transepithelial Electrical Resistance) measurement. All transwell assays were performed with transport buffer (Hanks' balanced salt solution with 10 mM HEPES and 25 mM D-glucose, 1.25 mM CaCl2, and 0.5 mM MgCl2) at pH 7.4 (buffered with 10 mM HEPES). Assays were performed with 1 μM test item (10 mM DMSO stock solution diluted in transport buffer) in

duplicate. hMDRI-MDCK Ⅱ cell monolayers are pre-incubated (at 37 ℃, in 5% CO_2 incubator) in transport media, all the apical sides and basolateral sides are pre-incubated for 40 min by 0.2 mL and 0.7 mL of the transport media. Transport study was performed by adding compound **47** or positive control (amprenavir) in transport buffer to donor wells and measuring appearance in receiver wells after a 90 min incubation at 37 °C. Bidirectional transport of test items in transfected MDCKII cells was determined in the presence or absence of the MDR1 inhibitor cyclosporine A to confirm the specificity of the transport in MDR1-MDCKII cells. For A to B directional transport, 0.2 mL of donor working solution with test articles or positive control (amprenavir) is added to the A compartment and then 0.7 mL of the transport media, as receiver working solution, is added to the B compartment. For B to A directional transport, 0.7 mL of donor working solution with test articles or positive control is added to the B compartment and 0.2 mL of the transport media, as receiver working solution, then to the A compartment. After the 90 min incubation period (37 ℃, in 5% CO_2 incubator), 80 μL of sample are taken from both donor and receiver compartments and added into 96-well assay plates, which were pre-added with 160 μL internal standard (IS) solution of acetonitrile. The plates are centrifuged (4000g, 10 min.) before LC-MS/MS analysis. The Apparent Permeability Coefficient P_{app} was calculated with the following equation:

$$P_{app} = \left(\frac{dM_r/d_t}{A \times C_0}\right)$$

where A is the surface area of the cell monolayer, C_0 is the initial concentration of compound applied to the donor chamber, t is time, M_r is the mass of compound appearing in the receiver compartment as a function of time, and dM_r/d_t is the flux of the compound across the cell monolayer.[61]

ACKNOWLEDGMENT

The authors are thankful to SIB Swiss Institute of Bioinformatics (www.sib.swiss) and its high-performance computing center (Vital-IT, www.vital-it.ch) for providing computational resources. This work was supported by the Commission for Technology and Innovation of the Swiss Confederation, CTI grants 15987.2 and 18012.1 to V.Z.

AUTHOR INFORMATION

Corresponding Authors

*(C.G.) Phone +41(0)91 9852152 claudio.giuliano@helsinn.com

*(C.P.) Phone +41(0)91 9851951 claudio.pietra@helsinn.com

*(V.Z.) Phone +41(0)21 6924082 vincent.zoete@sib.swiss

NOTES

The authors declare the following competing financial interest: C.P. C.G. S.G.R. and A.G. were Helsinn employees at the time of performing the study. J.W., Z.Z. and Y.C. were Sundia employees at the time of performing the study. F.L., Z.Y. and Y.Z. were HD Biosciences employees at the time of performing the study.

ABBREVIATIONS

GHSR, growth hormone secretagogue receptor; GPCR, G-protein coupled receptor; GHSR-IA, ghrelin receptor inverse agonists; SVM, support vector machine; MW, molecular weight; TPSA, topological surface area; CNS, central nervous system; WLOGP, in-house implementation of Wildman and Crippen log P; FLIPR, Fluorescent Imaging Plate Reader; IP-1, human inositol

phosphate accumulation assay; V_d, volume of distribution; P-gp, P-glycoprotein; F, oral bioavailability; $t_{1/2}$, plasma half-life ; FI, food intake

ASSOCIATED CONTENT

The Supporting Information is available free of charge on the ACS Publications website at DOI: XXX.

- Synthesis of additional compounds **8**, **11-14**, **19**, **20**, **22-45** (PDF)
- Molecular formula strings of all compounds (CSV)
- Predicted binding mode of **4** in GHSR model (PDB)
- Predicted binding mode of **8** in GHSR model (PDB)
- Predicted binding mode of **47** in GHSR model (PDB)

REFERENCES

(1) Howard, A. D.; Feighner, S. D.; Cully, D. F.; Arena, J. P. A Receptor in Pituitary and Hypothalamus That Functions in Growth Hormone Release. *Science* **1996**, *273* (5277), 974–977.

(2) McClure, K. F.; Jackson, M.; Cameron, K. O.; Kung, D. W.; Perry, D. A.; Orr, S. T. M.; Zhang, Y.; Kohrt, J.; Tu, M.; Gao, H.; Fernando, D. P.; Jones, R.; Erasga, N.; Wang, G.; Polivkova, J.; Jiao, W.; Swartz, R.; Ueno, H.; Bhattacharya, S. K.; Stock, I. A.; Varma, S.; Bagdasarian, V.; Perez, S.; Kelly-Sullivan, D.; Wang, R.; Kong, J.; Cornelius, P.; Michael, L.; Lee, E.; Janssen, A.; Steyn, S. J.; Lapham, K.; Goosen, T. Identification of Potent, Selective, CNS-Targeted Inverse Agonists of the Ghrelin Receptor. *Bioorg. Med. Chem. Lett.* **2013**, *23* (19), 5410–5414.

(3) Holst, B.; Cygankiewicz, A.; Jensen, T. H.; Ankersen, M.; Schwartz, T. W. High Constitutive Signaling of the Ghrelin Receptor--Identification of a Potent Inverse Agonist. *Mol. Endocrinol.* **2003**, *17* (11), 2201–2210.

(4) Kojima, M.; Hosoda, H.; Date, Y.; Nakazato, M.; Matsuo, H.; Kangawa, K. Ghrelin Is a Growth-Hormone-Releasing Acylated Peptide From Stomach. *Nature* **1999**, *402* (6762), 656–660.

(5) Maria A Bednarek; Scott D Feighner; Sheng-Shung Pong; Karen Kulju McKee; Donna L Hreniuk; Maria V Silva; Vivien A Warren; Andrew D Howard; Lex H Y Van der Ploeg, A.; Heck, J. V. Structure−Function Studies on the New Growth Hormone-Releasing Peptide, Ghrelin: Minimal Sequence of Ghrelin Necessary for Activation of Growth Hormone Secretagogue Receptor 1a. *J. Med. Chem.* **2000**, *43* (23), 4370–4376.

(6) Kojima, M.; Hosoda, H.; Matsuo, H.; Kangawa, K. Ghrelin: Discovery of the Natural Endogenous Ligand for the Growth Hormone Secretagogue Receptor. *Trends Endocrinol. Metab.* **2001**, *12* (3), 118–122.

(7) Tschöp, M.; Smiley, D. L.; Heiman, M. L. Ghrelin Induces Adiposity in Rodents. *Nature* **2000**, *407* (6806), 908–913.

(8) Shiiya, T.; Nakazato, M.; Mizuta, M.; Date, Y.; Mondal, M. S.; Tanaka, M.; Nozoe, S.-I.; Hosoda, H.; Kangawa, K.; Matsukura, S. Plasma Ghrelin Levels in Lean and Obese Humans and the Effect of Glucose on Ghrelin Secretion. *J. Clin. Endocr. Metab.* **2002**, *87* (1), 240–244.

(9) Isidro, M. L.; Cordido, F. Approved and Off-Label Uses of Obesity Medications, and Potential New Pharmacologic Treatment Options. *Pharmaceuticals* **2010**, *3* (1), 125–145.

(10) Dezaki, K.; Sone, H.; Koizumi, M.; Nakata, M.; Kakei, M.; Nagai, H.; Hosoda, H.; Kangawa, K.; Yada, T. Blockade of Pancreatic Islet–Derived Ghrelin Enhances Insulin Secretion to Prevent High-Fat Diet–Induced Glucose Intolerance. *Diabetes* **2006**, *55* (12), 3486–3493.

(11) Tong, J.; Prigeon, R. L.; Davis, H. W.; Bidlingmaier, M.; Kahn, S. E.; Cummings, D. E.; Tschöp, M. H.; D'Alessio, D. Ghrelin Suppresses Glucose-Stimulated Insulin Secretion and Deteriorates Glucose Tolerance in Healthy Humans. *Diabetes* **2010**, *59* (9), 2145–2151.

(12) Murata, M.; Okimura, Y.; Iida, K.; Matsumoto, M.; Sowa, H.; Kaji, H.; Kojima, M.; Kangawa, K.; Chihara, K. Ghrelin Modulates the Downstream Molecules of Insulin Signaling in Hepatoma Cells. *J. Biol. Chem.* **2002**, *277* (7), 5667–5674.

(13) Davies, J. S.; Kotokorpi, P.; Eccles, S. R.; Barnes, S. K.; Tokarczuk, P. F.; Allen, S. K.; Whitworth, H. S.; Guschina, I. A.; Evans, B. A. J.; Mode, A.; Zigman, J. M.; Wells, T. Ghrelin Induces Abdominal Obesity via GHS-R-Dependent Lipid Retention. *Mol. Endocrinol.* **2009**, *23* (6), 914–924.

(14) Theander-Carrillo, C.; Wiedmer, P.; Cettour-Rose, P.; Nogueiras, R.; Perez-Tilve, D.; Pfluger, P.; Castaneda, T. R.; Muzzin, P.; Schürmann, A.; Szanto, I.; Tschöp, M. H.; Rohner-Jeanrenaud, F. Ghrelin Action in the Brain Controls Adipocyte Metabolism. *J. Clin. Invest.* **2006**, *116* (7), 1983–1993.

(15) Cameron, K. O.; Bhattacharya, S. K.; Loomis, A. K. Small Molecule Ghrelin Receptor Inverse Agonists and Antagonists. *J. Med. Chem.* **2014**, *57* (21), 8671–8691.

(16) Pasternak, A.; Goble, S. D.; deJesus, R. K.; Hreniuk, D. L.; Chung, C. C.; Tota, M. R.; Mazur, P.; Feighner, S. D.; Howard, A. D.; Mills, S. G.; Yang, L. Discovery and Optimization of

Novel 4-[(Aminocarbonyl)Amino]-N-[4-(2-Aminoethyl)Phenyl]Benzenesulfonamide Ghrelin Receptor Antagonists. *Bioorg. Med. Chem. Lett.* **2009**, *19* (21), 6237–6240.

(17) Hoveyda, H.; Marsault, E.; Thomas, H.; Fraser, G.; Beaubien, S.; Mathieu, A.; Beignet, J.; Bonin, M. A.; Phoenix, S.; Drutz, D.; Peterson, M.; Beauchemin, S.; Brassard, M.; Vezina, M. *Preparation of Macrocyclic Ghrelin Receptor Antagonists and Inverse Agonists*; WO2011053821A1, 2011.

(18) McCoull, W.; Barton, P.; Broo, A.; Brown, A. J. H.; Clarke, D. S.; Coope, G.; Davies, R. D. M.; Dossetter, A. G.; Kelly, E. E.; Knerr, L.; MacFaul, P.; Holmes, J. L.; Martin, N.; Moore, J. E.; Morgan, D.; Newton, C.; Österlund, K.; Robb, G. R.; Rosevere, E.; Selmi, N.; Stokes, S.; Svensson, T. S.; Ullah, V. B. K.; Williams, E. J. Identification of Pyrazolo-Pyrimidinones as GHS-R1a Antagonists and Inverse Agonists for the Treatment of Obesity. *Med. Chem. Commun.* **2013**, *4* (2), 456–462.

(19) Bhattacharya, S. K.; Andrews, K.; Beveridge, R.; Cameron, K. O.; Chen, C.; Dunn, M.; Fernando, D. P.; Gao, H.; Hepworth, D.; Jackson, V. M.; Khot, V.; Kong, J.; Kosa, R. E.; Lapham, K.; Loria, P. M.; Londregan, A. T.; McClure, K. F.; Orr, S. T. M.; Patel, J.; Rose, C.; Saenz, J.; Stock, I. A.; Storer, G.; VanVolkenburg, M.; Vrieze, D.; Wang, G.; Xiao, J.; Zhang, Y. Discovery of PF-5190457, a Potent, Selective, and Orally Bioavailable Ghrelin Receptor Inverse Agonist Clinical Candidate. *ACS Med. Chem. Lett.* **2014**, *5* (5), 474–479.

(20) Maingot, M.; Blayo, A.-L.; Denoyelle, S.; M'Kadmi, C.; Damian, M.; Mary, S.; Gagne, D.; Sanchez, P.; Aicher, B.; Schmidt, P.; Müller, G.; Teifel, M.; Günther, E.; Marie, J.; Banères, J.-L.; Martinez, J.; Fehrentz, J.-A. New Ligands of the Ghrelin Receptor Based on the 1,2,4-

Triazole Scaffold by Introduction of a Second Chiral Center. *Bioorg. Med. Chem. Lett.* **2016**, *26* (10), 2408–2412.

(21) McCoull, W.; Barton, P.; Brown, A.; Bowker, S.; Cameron, J.; Clarke, D.; Davies, R.; Dossetter, A.; Ertan, A.; Fenwick, M.; Green, C.; Holmes, J.; Martin, N.; Masters, D.; Moore, J.; Newcombe, N.; Newton, C.; Pointon, H.; Robb, G. R.; Sheldon, C.; Stokes, S.; Morgan, D. Identification, Optimization and Pharmacology of Acylurea GHS-R1a Inverse Agonists. *J. Med. Chem.* **2014**, *57* (14), 6128–6140.

(22) Takahashi, B.; Funami, H.; Iwaki, T.; Maruoka, H.; Shibata, M.; Koyama, M.; Nagahira, A.; Kamiide, Y.; Kanki, S.; Igawa, Y.; Muto, T. Bioorganic & Medicinal Chemistry. *Bioorg. Med. Chem.* **2015**, *23* (15), 4792–4803.

(23) Ertl, P.; Rohde, B.; Selzer, P. Fast Calculation of Molecular Polar Surface Area as a Sum of Fragment-Based Contributions and Its Application to the Prediction of Drug Transport Properties. *J. Med. Chem.* **2000**, *43* (20), 3714–3717.

(24) Daina, A.; Michielin, O.; Zoete, V. SwissADME: a Free Web Tool to Evaluate Pharmacokinetics, Drug-Likeness and Medicinal Chemistry Friendliness of Small Molecules. *Sci. Rep.* **2017**, *7*, 42717.

(25) White, H. K.; Petrie, C. D.; Landschulz, W.; MacLean, D.; Taylor, A.; Lyles, K.; Wei, J. Y.; Hoffman, A. R.; Salvatori, R.; Ettinger, M. P.; Morey, M. C.; Blackman, M. R.; Merriam, G. R. Effects of an Oral Growth Hormone Secretagogue in Older Adults. *J. Clin. Endocr. Metab.* **2009**, *94* (4), 1198–1206.

(26) Banks, W. A.; Tschöp, M.; Robinson, S. M.; Heiman, M. L. Extent and Direction of Ghrelin Transport Across the Blood-Brain Barrier Is Determined by Its Unique Primary Structure. *J. Pharmacol. Exp. Ther.* **2002**, *302* (2), 822–827.

(27) Arnold, M.; Mura, A.; Langhans, W.; Geary, N. Gut Vagal Afferents Are Not Necessary for the Eating-Stimulatory Effect of Intraperitoneally Injected Ghrelin in the Rat. *J. Neurosci.* **2006**, *26* (43), 11052–11060.

(28) Mason, B. L.; Wang, Q.; Zigman, J. M. The Central Nervous System Sites Mediating the Orexigenic Actions of Ghrelin. *Annu Rev Physiol.* **2014**, *76* (1), 519–533.

(29) Abegg, K.; Bernasconi, L.; Hutter, M.; Whiting, L.; Pietra, C.; Giuliano, C.; Lutz, T. A.; Riediger, T. Ghrelin Receptor Inverse Agonists as a Novel Therapeutic Approach Against Obesity-Related Metabolic Disease. *Diabetes Obes. Metab.* **2017**, *19* (12), 1740–1750.

(30) Kong, J.; Chuddy, J.; Stock, I. A.; Loria, P. M.; Straub, S. V.; Vage, C.; Cameron, K. O.; Bhattacharya, S. K.; Lapham, K.; McClure, K. F.; Zhang, Y.; Jackson, V. M. Pharmacological Characterization of the First in Class Clinical Candidate PF-05190457: a Selective Ghrelin Receptor Competitive Antagonist with Inverse Agonism That Increases Vagal Afferent Firing and Glucose-Dependent Insulin Secretion Ex Vivo. *Br. J. Pharmacol.* **2016**, *173* (9), 1452–1464.

(31) Callaghan, B.; Furness, J. B. Novel and Conventional Receptors for Ghrelin, Desacyl-Ghrelin, and Pharmacologically Related Compounds. *Pharmacol. Rev.* **2014**, *66* (4), 984–1001.

(32) Denney, W. S.; Sonnenberg, G. E.; Carvajal Gonzalez, S.; Tuthill, T.; Jackson, V. M. Pharmacokinetics and Pharmacodynamics of PF-05190457: the First Oral Ghrelin Receptor

Inverse Agonist to Be Profiled in Healthy Subjects. *Br. J. Clin. Pharmacol.* **2017**, *83* (2), 326–338.

(33) Wildman, S. A.; Crippen, G. M. Prediction of Physicochemical Parameters by Atomic Contributions. *J. Chem. Inf. Comput. Sci.* **1999**, *39* (5), 868–873.

(34) Giuliano, C.; Garcia Rubio, S.; Daina, A.; Guainazzi, A.; Pietra, C. *P-Substituted Asymmetric Ureas and Medical Uses Thereof*; WO2015134839A1, 2015.

(35) Zoete, V.; Schuepbach, T.; Bovigny, C.; Chaskar, P.; Daina, A.; Röhrig, U. F.; Michielin, O. Attracting Cavities for Docking. Replacing the Rough Energy Landscape of the Protein by a Smooth Attracting Landscape. *J. Comput. Chem.* **2015**, *37* (4), 437–447.

(36) Feighner, S. D.; Howard, A. D.; Prendergast, K.; Palyha, O. C.; Hreniuk, D. L.; Nargund, R.; Underwood, D.; Tata, J. R.; Dean, D. C.; Tan, C. P.; McKee, K. K.; Woods, J. W.; Patchett, A. A.; Smith, R. G.; Van der Ploeg, L. H. T. Structural Requirements for the Activation of the Human Growth Hormone Secretagogue Receptor by Peptide and Nonpeptide Secretagogues. *Mol. Endocrinol.* **1998**, *12* (1), 137–145.

(37) Holst, B.; Frimurer, T. M.; Mokrosinski, J.; Halkjaer, T.; Cullberg, K. B.; Underwood, C. R.; Schwartz, T. W. Overlapping Binding Site for the Endogenous Agonist, Small-Molecule Agonists, and Ago-Allosteric Modulators on the Ghrelin Receptor. *Mol. Pharmacol.* **2009**, *75* (1), 44–59.

(38) Sivertsen, B.; Lang, M.; Frimurer, T. M.; Holliday, N. D.; Bach, A.; Els, S.; Engelstoft, M. S.; Petersen, P. S.; Madsen, A. N.; Schwartz, T. W.; Beck-Sickinger, A. G.; Holst, B. Unique

Interaction Pattern for a Functionally Biased Ghrelin Receptor Agonist. *J. Biol. Chem.* **2011**, *286* (23), 20845–20860.

(39) Els, S.; Schild, E.; Petersen, P. S.; Kilian, T.-M.; Mokrosinski, J.; Frimurer, T. M.; Chollet, C.; Schwartz, T. W.; Holst, B.; Beck-Sickinger, A. G. An Aromatic Region to Induce a Switch Between Agonism and Inverse Agonism at the Ghrelin Receptor. *J. Med. Chem.* **2012**, *55* (17), 7437–7449.

(40) Holst, B.; Holliday, N. D.; Bach, A.; Elling, C. E.; Cox, H. M.; Schwartz, T. W. Common Structural Basis for Constitutive Activity of the Ghrelin Receptor Family. *J. Biol. Chem.* **2004**, *279* (51), 53806–53817.

(41) Mokrosinski, J.; Frimurer, T. M.; Sivertsen, B.; Schwartz, T. W.; Holst, B. Modulation of Constitutive Activity and Signaling Bias of the Ghrelin Receptor by Conformational Constraint in the Second Extracellular Loop. *J. Biol. Chem.* **2012**, *287* (40), 33488–33502.

(42) Holst, B.; Mokrosinski, J.; Lang, M.; Brandt, E.; Nygaard, R.; Frimurer, T. M.; Beck-Sickinger, A. G.; Schwartz, T. W. Identification of an Efficacy Switch Region in the Ghrelin Receptor Responsible for Interchange Between Agonism and Inverse Agonism. *J. Biol. Chem.* **2007**, *282* (21), 15799–15811.

(43) Costantino, L.; Barlocco, D. Ghrelin Receptor Modulators: a Patent Review (2011 - 2014). *Expert Opin. Ther. Pat.* **2014**, *24* (9), 1007–1019.

(44) Garcia Rubio, S.; Pietra, C.; Giuliano, C.; Li, Z. *Asymmetric Ureas and Medical Uses Thereof*; WO2012116176A2, 2012.

(45) Smith, R. G.; Cheng, K.; Schoen, W. R.; Pong, S. S.; Hickey, G.; Jacks, T.; Butler, B.; Chan, W. W.; Chaung, L. Y.; Judith, F. A Nonpeptidyl Growth Hormone Secretagogue. *Science* **1993**, *260* (5114), 1640–1643.

(46) Delaney, J. S. ESOL: Estimating Aqueous Solubility Directly From Molecular Structure. *J. Chem. Inf. Comput. Sci.* **2004**, *44* (3), 1000–1005.

(47) Bonomi, P.; Temel, J.; Currow, D.; Fearon, K.; Gleich, L.; Yan, Y.; Friend, J.; Abernethy, A. Anamorelin for the Treatment of Cancer Anorexia-Cachexia in Advanced NSCLC Patients: Results From ROMANA 1, a Pivotal Phase 3 Study. *Int. J. Radiat. Oncol. Biol. Phys.* **2014**, *90* (5), S3.

(48) Bhattacharya, S. K.; Cameron, K. O. K.; Fernando, D. P.; Kung, D. W.; Londregan, A. T.; McClure, K. F.; Simila, S. T. M. *2,3-Dihydro-1H-Inden-1-Yl-2,7-Diazaspiro[3.6]Nonane Derivatives as Ghrelin Receptor Antagonists or Inverse Agonists and Their Preparation and Use for the Treatment of Ghrelin Receptor-Mediated Diseases.*; WO2011114271A1, 2011.

(49) Shioiri, T.; Ninomiya, K.; Yamada, S. Diphenylphosphoryl Azide. New Convenient Reagent for a Modified Curtius Reaction and for Peptide Synthesis. *J. Am. Chem. Soc.* **1972**, *94* (17), 6203–6205.

(50) Lott, R. S.; Chauhan, V. S.; Stammer, C. H. Trimethylsilyl Iodide as a Peptide Deblocking Agent. *Chem. Commun.* **1979**, *11* (11), 495–496.

(51) Palagiano, F.; Arenare, L.; Luraschi, E.; de Caprariis, P.; Abignente, E.; D'Amico, M.; Filippelli, W.; Rossi, F. Research on Heterocyclic Compounds. XXXIV. Synthesis and SAR

Study of Some Imidazo[2,1-B]Thiazole Carboxylic and Acetic Acids with Antiinflammatory and Analgesic Activities. *Eur. J. Med. Chem.* **1995**, *30* (11), 901–909.

(52) Pieper, U.; Webb, B. M.; Dong, G. Q.; Schneidman-Duhovny, D.; Fan, H.; Kim, S. J.; Khuri, N.; Spill, Y. G.; Weinkam, P.; Hammel, M.; Tainer, J. A.; Nilges, M.; Sali, A. ModBase, a Database of Annotated Comparative Protein Structure Models and Associated Resources. *Nucleic Acids Res.* **2014**, *42* (D1), D336–D346.

(53) Brooks, B. R.; Brooks, C. L.; MacKerell, A. D.; Nilsson, L.; Petrella, R. J.; Roux, B.; Won, Y.; Archontis, G.; Bartels, C.; Boresch, S.; Caflisch, A.; Caves, L.; Cui, Q.; Dinner, A. R.; Feig, M.; Fischer, S.; Gao, J.; Hodoscek, M.; Im, W.; Kuczera, K.; Lazaridis, T.; Ma, J.; Ovchinnikov, V.; Paci, E.; Pastor, R. W.; Post, C. B.; Pu, J. Z.; Schaefer, M.; Tidor, B.; Venable, R. M.; Woodcock, H. L.; Wu, X.; Yang, W.; York, D. M.; Karplus, M. CHARMM: the Biomolecular Simulation Program. *J. Comput. Chem.* **2009**, *30* (10), 1545–1614.

(54) MacKerell, A. D.; Bashford, D.; Bellott; Dunbrack, R. L.; Evanseck, J. D.; Field, M. J.; Fischer, S.; Gao, J.; Guo, H.; Ha, S.; Joseph-McCarthy, D.; Kuchnir, L.; Kuczera, K.; Lau, F. T. K.; Mattos, C.; Michnick, S.; Ngo, T.; Nguyen, D. T.; Prodhom, B.; Reiher, W. E.; Roux, B.; Schlenkrich, M.; Smith, J. C.; Stote, R.; Straub, J.; Watanabe, M.; Wiórkiewicz-Kuczera, J.; Yin, D.; Karplus, M. All-Atom Empirical Potential for Molecular Modeling and Dynamics Studies of Proteins. *J. Phys. Chem. B* **1998**, *102* (18), 3586–3616.

(55) Subramaniam, S.; Senes, A. An Energy-Based Conformer Library for Side Chain Optimization: Improved Prediction and Adjustable Sampling. *Proteins* **2012**, *80* (9), 2218–2234.

(56) Cortes, C.; Vapnik, V. Support-Vector Networks. *Mach Learn* **1995**, *20* (3), 273–297.

(57) Wang, R.; Fu, Y.; Lai, L. A New Atom-Additive Method for Calculating Partition Coefficients. *J. Chem. Inf. Comput. Sci.* **1997**, *37* (3), 615–621.

(58) Baell, J. B.; Holloway, G. A. New Substructure Filters for Removal of Pan Assay Interference Compounds (PAINS) From Screening Libraries and for Their Exclusion in Bioassays. *J. Med. Chem.* **2010**, *53* (7), 2719–2740.

(59) *Guide for the Care and Use of Laboratory Animals*, 7 ed.; Institute of Laboratory Animal Resources, National Research Council: Washington, DC, 1996.

(60) Obach, R. S. Prediction of Human Clearance of Twenty-Nine Drugs From Hepatic Microsomal Intrinsic Clearance Data: an Examination of in Vitro Half-Life Approach and Nonspecific Binding to Microsomes. *Drug Metab. Dispo.* **1999**, *27* (11), 1350–1359.

(61) Feng, B.; Mills, J. B.; Davidson, R. E.; Mireles, R. J.; Janiszewski, J. S.; Troutman, M. D.; de Morais, S. M. In Vitro P-Glycoprotein Assays to Predict the in Vivo Interactions of P-Glycoprotein with Drugs in the Central Nervous System. *Drug Metab. Dispo.* **2008**, *36* (2), 268–275.

Table of Contents graphic (high-res TIFF uploaded separately)

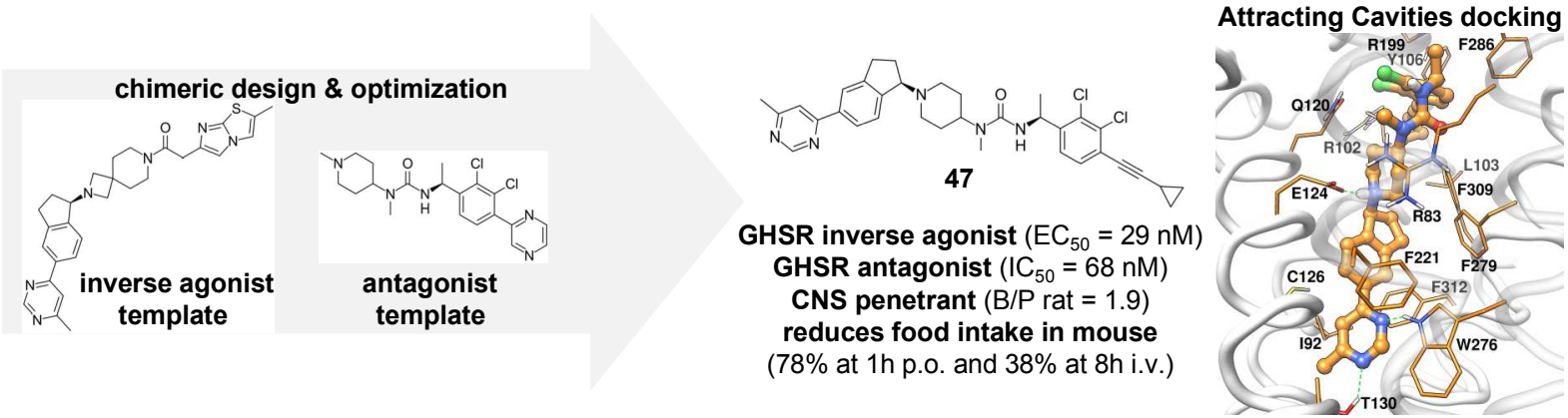

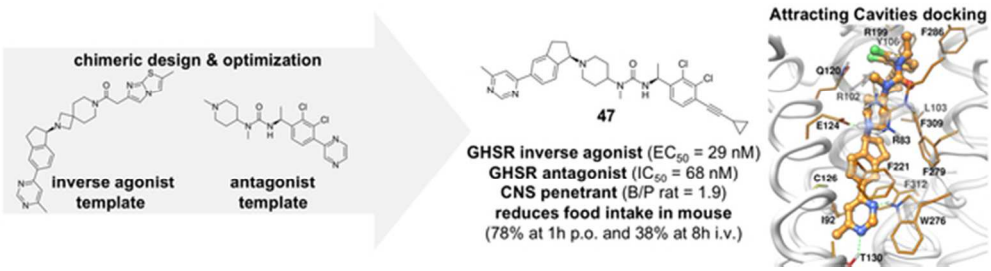

TOC graphic (high-resolution)

55x14mm (300 x 300 DPI)